

1           **A *trans*-acting long non-coding RNA represses flowering in *Arabidopsis***

2           Yu Jin<sup>1</sup>, Maxim Ivanov<sup>1</sup>, Anna Nelson Dittrich<sup>2</sup>, Andrew D. L. Nelson<sup>2</sup> and Sebastian Marquardt<sup>1\*</sup>

3           \*Correspondence: sebastian.marquardt@plen.ku.dk

4           <sup>1</sup>Department of Plant and Environmental Sciences, Copenhagen Plant Science Centre, University of  
5           Copenhagen, Frederiksberg, Denmark

6           <sup>2</sup>Boyce Thompson Institute, Cornell University, Ithaca, NY, USA

7

8           **Keywords**

9           lncRNA, *FLAIL*, *trans*-acting, chromatin binding, flowering regulation, ChIRP-seq

10

11           **Abstract**

12           Eukaryotic genomes give rise to thousands of long non-coding RNAs (lncRNAs), yet the purpose of  
13           lncRNAs remains largely enigmatic. Functional characterization of lncRNAs is challenging due to  
14           multiple orthogonal hypothesis for molecular activities of lncRNA loci. Here, we identified a **flowering**  
15           **associated intergenic lncRNA (*FLAIL*)** that represses flowering in *Arabidopsis*. An allelic series of *flail*  
16           loss-of-function mutants generated by CRISPR/Cas9 and T-DNA mutagenesis showed an early  
17           flowering phenotype. Gene expression analyses in *flail* mutants revealed differentially expressed  
18           genes linked to the regulation of flowering. A genomic rescue fragment of *FLAIL* introduced in *flail*  
19           mutants complemented gene expression defects and early flowering, consistent with *trans*-acting  
20           effects of the *FLAIL* RNA. Knock-down of *FLAIL* RNA levels using the artificial microRNA approach  
21           revealed an early flowering phenotype shared with genomic mutations, indicating a *trans*-acting role  
22           of *FLAIL* RNA in the repression of flowering time. Genome-wide detection of *FLAIL*-DNA interactions  
23           by ChIRP-seq suggested that *FLAIL* may directly bind genomic regions. *FLAIL* bound to genes  
24           involved in regulation of flowering that were differentially expressed in *flail*, consistent with the  
25           interpretation of *FLAIL* as a *trans*-acting lncRNA directly shaping gene expression. Our findings  
26           highlight *FLAIL* as a *trans*-acting lncRNA that affects flowering in *Arabidopsis*, likely through mediating  
27           transcriptional regulation of genes directly bound by *FLAIL*.

28

29           **Background**

30           The purpose of DNA sequences that do not encode proteins represents an open question in the  
31           biology of genomes. It is now clear that RNA polymerase II (RNAPII) converts non-coding DNA into  
32           non-coding RNA genome-wide [1]. Long non-coding RNAs (lncRNAs) are key products of ubiquitous  
33           RNAPII transcription in the non-coding genome [2]. Non-coding DNA engaged in lncRNA production  
34           may function through various molecular mechanisms, ranging from roles as DNA elements, RNAs,  
35           the act of transcription and small peptides [3, 4]. This wide range of possible cellular roles affects  
36           strategies to elucidate their functions experimentally [5]. Functional characterization of DNA elements  
37           benefits from a high-quality annotation of lncRNAs in genomes [6]. Integration of several orthogonal

38 transcriptomic data offers an opportunity to inform on the precise location of various lncRNA subtypes  
39 and alternative lncRNA isoforms from a single locus [6]. Experimental avenues to abolish specific  
40 lncRNA isoforms may trigger the generation of alternative isoforms that may partially substitute for  
41 functions, calling for a multi-faceted functional characterization of lncRNA loci [7, 8]. The resulting  
42 RNA molecules, but also the act of transcription generating lncRNA can regulate the expression of  
43 neighboring genes [9]. The act of transcription from an upstream lncRNA locus may trigger gene  
44 activation of the downstream, or gene repression, for instance by transcriptional interference [9].  
45 Ribosome profiling (Ribo-seq) may suggest small open reading frames (sORFs) of the lncRNA loci  
46 [3]. Notably, lncRNA association with ribosomes may indicate either ribosome-coupled RNA  
47 degradation or translation [3]. Collectively, the broad range of candidate hypotheses by which lncRNA  
48 loci may play functional roles call for multiple approaches to distinguish alternative molecular  
49 mechanisms [10].

50 LncRNAs may regulate nearby genes in *cis* or distant genes in *trans* [11-13]. Compared to *cis*-acting  
51 lncRNAs, relatively fewer functions of *trans*-acting lncRNAs have been clarified [4]. A key experiment  
52 to distinguish between *cis*-acting and *trans*-acting mechanisms is to test phenotypic complementation  
53 of lncRNA loss-of-function mutants by lncRNA expression from a different genomic region [4]. *Trans*-  
54 acting lncRNAs regulate distant genes via different mechanisms [11], for example, through chromatin  
55 targeting of lncRNAs to fine tune chromatin architecture resulting in an altered transcriptional output  
56 [14]. Nevertheless, functional characterization of *trans*-acting lncRNAs remains a key knowledge gap  
57 to understand the regulatory contributions of the non-coding genome.

58 In plants, an increasing number of lncRNA loci have been implicated in the regulation of flowering  
59 time [15-20]. Flowering time represents a developmental transition of plants that is key for  
60 reproductive success. Genetic and environmental factors, for example, altered internal secondary  
61 metabolites (e.g. lignin), extended cold periods (i.e. vernalization) or day length (i.e. photoperiod),  
62 help plants to align flowering with favorable conditions [21-23]. Vernalization-induced flowering  
63 associates with several lncRNAs such as *COOLAIR*, *COLDAIR*, *ANTISENSE LONG (ASL)*, and  
64 *COLDWRAP* that in *cis* repress gene expression of *FLOWERING LOCUS C (FLC)*, a key flowering  
65 repressor at different stages of vernalization [24-27]. The contribution of *trans*-acting lncRNAs to the  
66 regulation of flowering time is currently unclear.

67 Here, we characterized the lncRNA locus *FLAIL* in *Arabidopsis* that gives rise to several RNA isoforms.  
68 Genomic mutations and strand-specific RNA repression provided evidence that *FLAIL* sense lncRNA  
69 repressed flowering. Genetic complementation data supported a *trans*-acting role of *FLAIL* in the  
70 regulation of flowering genes. *FLAIL* RNA bound the chromatin of flowering-related target genes that  
71 were differentially expressed in *flail* mutants, arguing for direct effects of *FLAIL* in flowering gene  
72 regulation. In summary, our data suggest flowering regulation through effects on gene expression by  
73 chromatin association of the *trans*-acting RNA *FLAIL*.

75 **Results**

76 **Characterization of the *FLAIL* locus**

77 *FLAIL* was annotated as a lncRNA in the TAIR [28] and GreeNC [29] databases and mapped as a  
78 single exon to chromosome 2 in *Arabidopsis* (Fig. 1A). Consistently, Nanopore RNA-seq data of  
79 chromatin-associated RNAs provided no evidence for splicing at the *FLAIL* locus [30] (Fig. S1A).  
80 Additionally, plaNET-seq used for genome-wide profiling of nascent RNA polymerase II (RNAPII)  
81 transcription [31], identified both sense and antisense isoforms at the *FLAIL* locus (Fig. 1A). We  
82 obtained additional information by examining RNA 5'-end mapping by TSS-seq [32] and simultaneous  
83 RNA 5'- and 3'-end mapping by TIF-seq [33] in the mutant of the nuclear exosome component *HUA*  
84 *ENHANCER2* (i.e. *hen2-2*). These data confirmed that the *FLAIL* locus was transcribed on both  
85 strands, since sense and antisense *FLAIL* transcripts were detected. Moreover, RNA isoforms derived  
86 from *FLAIL* were 5'-end capped, 3'-end polyadenylated and degraded by the nuclear exosome in  
87 *Arabidopsis* (Fig. 1A). To assess the protein-coding potential of *FLAIL* RNAs, we used the Coding  
88 Potential Calculator (CPC2) [34] and Coding-NonCoding Identifying Tool (CNIT) [35]. These analyses  
89 revealed poor coding potential of the lncRNA *FLAIL*, similar to other well-known ncRNAs (*18sRNA*,  
90 *U6*, *ELENA1*, *SVALKA*) [36, 37], but much lower than the protein coding potential of *UBIQUITIN* (*UBQ*)  
91 mRNA (Fig. 1B). Finally, an analysis of translation start sites in *FLAIL* RNAs suggested poor protein  
92 coding potential, well below the 0.5 threshold predicted for protein start codon as determined by the  
93 NetStart software package [38] (Fig. S2). Nevertheless, Ribo-seq [39, 40] data indicated ribosome  
94 association of *FLAIL* RNAs. This ribosome association could be consistent with translation of two  
95 sORFs with ~9 amino acids, or ribosome-mediated RNA degradation (Fig. S1B) [39]. In summary, the  
96 *FLAIL* locus harbors both sense and antisense lncRNA isoforms.

97 Even though lncRNAs show relatively poor sequence conservation [41], *trans*-acting lncRNAs may  
98 show signatures of conservation across species [42]. We identified a match in the genome of  
99 *Camelina sativa* on chromosome 17 (Fig. S3A). *Camelina*, like *Arabidopsis*, is in the Brassicaceae  
100 and last shared a common ancestor with *Arabidopsis* ~ 18 million years ago [43]. Reciprocal blast  
101 searches narrowed down a microhomology region between the sense *FLAIL* 3'-end in *Arabidopsis*  
102 and a non-coding DNA region near the *Camelina* gene *Csa17g011930*. In turn this region in *Camelina*  
103 is syntenic to a genomic region in *Arabidopsis* surrounding the *At1G08480* locus (Fig. S3A). Indeed,  
104 we successfully detected the existence of genomic *FLAIL*-like non-coding DNA by PCR amplification  
105 (Fig. S3C). We next performed RT-PCR targeting the *FLAIL*-like non-coding DNA region to examine  
106 RNA expression in *Camelina sativa* leaves and seedlings (Fig. S3B-C). Our data are consistent with  
107 the expression of RNA from the *FLAIL*-like non-coding DNA region in *Camelina sativa*, even though  
108 we detected noticeably weaker expression compared to *Arabidopsis* *FLAIL* expression in equivalent  
109 experimental conditions. In conclusion, our comparative genomic analysis identified a candidate  
110 *FLAIL*-like non-coding DNA region in Brassicaceae with signatures of RNA expression.

111

## 112 ***FLAIL* characterizes a *trans*-acting lncRNA repressing flowering**

113 To address the function of *FLAIL* in *Arabidopsis*, we used CRISPR/Cas9 technology with paired  
114 sgRNAs to generate two different *flail* knockout mutants with deletion fragments of 229 bp (*flail1*) [44],  
115 and 343 bp (*flail2*) (Fig. S4A-E). We also obtained a mutant line SAIL\_645\_C03 (*flail3*) carrying a T-  
116 DNA insertion at the 3'-end of sense *FLAIL* locus (Fig. S4A, F). All three mutants reduced the  
117 expression of sense and antisense *FLAIL* transcripts as detected by RT-qPCR, suggesting that they  
118 reduced the bioavailability of *FLAIL* isoforms (Fig. 1C-D). All three *flail* mutants flowered earlier than  
119 wild type (Fig. 1E-F). Our genetic data thus revealed a link between non-coding transcription at the  
120 *FLAIL* locus and flowering time.

121 To test which transcript of *FLAIL* was linked to the observed phenotype of the *flail* mutant we  
122 performed a complementation test. We transformed a DNA fragment encoding either sense or  
123 antisense *FLAIL* driven by the corresponding native promoter into the *flail3* mutant background with  
124 *GUS* driven by *35S* promoter as a control (Fig. 2A). Importantly, the constructs carried the *NOS*  
125 terminator that largely abolished initiation of antisense transcription [8, 37, 45]. We selected *flail3* for  
126 complementation because *FLAIL* disruption by T-DNA insertion at the 3'-end left potential sORF  
127 regions at the 5'-end intact (Fig. S4A). We selected two representative homozygous single locus  
128 insertion lines for each transformed construct (*flail3 pFLAIL:gFLAIL18/88* and *flail3*  
129 *pasFLAIL:gasFLAIL18/39*) that expressed sense and antisense *FLAIL* at levels slightly higher than or  
130 similar to wild type (Fig. 2B-C). However, only exogenous expression of sense *FLAIL* rescued the  
131 early flowering phenotype of the *flail3* mutant (Fig. 2D-E), suggesting that the early flowering of  
132 the *flail* mutant was caused by the disruption of the sense *FLAIL* transcript isoform. In *Arabidopsis*,  
133 transgene insertion is non-targeted. We thus reasoned that complementation argued for the capability  
134 of sense *FLAIL* to act from a different genomic location, presumably as a *trans*-acting lncRNA. This  
135 hypothesis predicts that knock-down of sense *FLAIL* RNA should result in equivalent effects as  
136 genomic mutations. To test this hypothesis, we employed strand-specific RNA repression using  
137 artificial microRNAs (amiRNAs) [46]. We generated two amiRNA targets (*amiR-FLAIL-11* and *amiR-*  
138 *FLAIL-12*) (Additional file1: Fig. S5A), both exhibiting strongly reduced sense *FLAIL* transcription  
139 (Additional file1: Fig. S5B) and similar effects on flowering as genomic mutations (Additional file1: Fig.  
140 S5C-D). In conclusion, our experimental data indicate that the sense *FLAIL* lncRNA represses  
141 flowering through a *trans*-acting mechanism.

142

## 143 ***FLAIL* lncRNA binding to chromatin regions promotes the expression of selected flowering 144 repressors**

145 Early flowering in *Arabidopsis* may be associated with altered expression of flowering-related genes.  
146 To gain insight into the molecular basis of *FLAIL*-mediated regulation of flowering time, we determined

147 the transcriptional profiles of two-week old seedlings for wild type, *flail3*, and *flail3 pFLAIL:gFLAIL* with  
148 at least two independent replicates using stranded RNA-seq. Since the early flowering time effect in  
149 *flail3* could be rescued by *pFLAIL:gFLAIL*, we reasoned that this experimental setup may be suitable  
150 to identify gene expression changes directly correlated with sense *FLAIL* expression. Compared to  
151 wild type, 1221 differentially expressed genes (DEGs) were called by DESeq2 with at least two-fold  
152 change (adjusted *p* value < 0.05; Table S1), with 419 up-regulated and 802 down-regulated genes in  
153 *flail3* mutants. Almost half of these transcriptional differences in *flail3* reverted to wild-type expression  
154 level by exogenous expression of the *FLAIL* sense RNA into *flail3* mutants, including the *FLAIL*  
155 lncRNA itself (Fig. S6A and Fig. S7F, Table S2). We next focused on functional annotations of genes  
156 associated with the process of flowering [47]. Among the DEGs in *flail3*, we identified twenty genes  
157 linked to flowering (Fig. S6A). Expression of most of them were fully (eight) or partially (five) rescued  
158 by the expression of *pFLAIL:gFLAIL* (Fig. 3A-E, Fig. 4E-H, Fig. S6B, S7A-E and S9B, D). In  
159 conclusion, our transcriptomic data indicate potential targets for the *trans*-acting lncRNA *FLAIL*.  
160 The reversible effect on flowering gene expression upon re-introduction of *pFLAIL:gFLAIL* argued for  
161 a direct effect of the *FLAIL* lncRNA. To identify where *FLAIL* bound chromatin regions, we performed  
162 chromatin isolation by RNA purification (ChIRP) of endogenous *FLAIL* followed by DNA-seq (*FLAIL*  
163 ChIRP-seq). We targeted sense *FLAIL* by two non-overlapping antisense oligonucleotide pools (Even  
164 and Odd probes, Fig. 4A bottom) tiled along the entire *FLAIL* transcript sequence compared to an  
165 oligonucleotide pool against the *LUCIFERASE* (*LUC*) mRNA as control that is not expressed in our  
166 strains. We efficiently captured the endogenous *FLAIL* RNA from chromatin compared to the  
167 unrelated *UBQ* mRNA (Fig. 4B). Moreover, *LUC*-specific probes did not enrich *FLAIL*, suggesting the  
168 specificity of RNA affinity purification in our assay conditions (Fig. 4B). After isolating DNA fragments  
169 associated with the *FLAIL*-containing complex, we assessed the genome-wide occupancy of *FLAIL*  
170 at high resolution by ChIRP-seq, followed by peak calling using CCAT3.0 [48]. Only peaks that  
171 occurred at target genes from both even and odd probe pools, but not from two or more independent  
172 experiments of Luc pools were considered significantly enriched (Fig. S8A). This analysis strategy  
173 allowed us to identify 210 target genes of *FLAIL* (Table S3). We observed a strong enrichment for the  
174 *FLAIL* locus by both ChIRP-seq (Fig. 4A, top) and ChIRP-qPCR (Fig. 4C). We noted that the *FLAIL*  
175 locus represented the only locus where we could expect binding, thus validating our identification  
176 strategy of genomic *FLAIL* binding. We analyzed the overlap between genes which were differentially  
177 expressed in the RNA-seq experiment and those genes that showed statistically significant *FLAIL*  
178 binding by ChIRP-seq (Fig. 4F). We identified twelve genes matching both criteria. At these targets,  
179 chromatin binding by *FLAIL* was linked to corresponding changes of gene expression, arguing for  
180 direct effects of *FLAIL* binding on gene expression. Four of these genes were functionally connected  
181 to flowering: *CIRCADIAN 1* (*CIR1*), *LACCASE 8* (*LAC8*), *PECTIN LYASE-LIKE 25* (*PLL25*) and  
182 *PHOSPHOETHANOLAMINE N-METHYLTRANSFERASE 3* (*NMT3*) (Table S4). All four flowering  
183 genes were transcriptionally down-regulated in *flail3* (Fig. 4D-E and 4G-H, Fig. S9A-D, Table S1).

184 However, the complementation construct failed to restore *NMT3* expression, arguing against a direct  
185 effect here (Fig. S9A-B, Table S2). A detailed examination revealed that *PLL25* regulates flower  
186 morphology rather than flowering time [49], arguing against effects on flowering time through mis-  
187 regulation of this gene [50, 51]. On the other hand, *cir1* [52] and *lac8* [53] mutants displayed early  
188 flowering phenotypes. These data suggest repression of *CIR1* and *LAC8* as candidate molecular  
189 hypothesis to explain the early flowering time phenotype in *flail* [52, 53]. In conclusion, our data  
190 suggest that *FLAIL* sense RNA represses flowering through inhibiting expression of the direct *FLAIL*  
191 targets *CIR1* and *LAC8*, consistent with a model where gene expression changes regulating flowering  
192 are mediated by interactions of the *trans*-acting lncRNA *FLAIL* with the genome (Fig. 4I).

193

## 194 Discussion

195

### 196 *FLAIL* functions in flowering time

197 In this study, we report repression of flowering time by the *trans*-acting lncRNA *FLAIL*. While many  
198 lncRNAs affect flowering regulation, the molecular mechanisms remain largely unclear [15-20].  
199 Previously characterized lncRNAs including *COOLAIR*, *COLDAIR*, *ASL*, *COLDWRAP*, and *MAS* are  
200 transcribed from the flowering genes *FLC* or *MAF4* to locally affect their coding gene expression in  
201 *cis* [20, 24, 27, 54, 55]. We note that the *FLAIL* 3'-end resides approximately 130 bp upstream of the  
202 5' UTR region of the *PORCUPINE* (*PCP*, also called *Sm protein E1*, *SME1*) gene, and *pcp/sme1*  
203 mutants flower early [56, 57]. We failed to find evidence for the hypothesis that *FLAIL* may affect  
204 flowering through *PCP* by a *cis*-acting mechanism. *FLAIL* neither regulates *PCP* expression nor  
205 shows overlapping effects on gene expression (Table S1 and S5-7, Fig. S10A-D).

206 In contrast, our work identifies a *trans*-acting *FLAIL* that represses flowering and binds multiple  
207 genomic loci. We thus favor the interpretation that *FLAIL* binding to other genomic regions explains  
208 the phenotypic effects of the mutants. For instance, *FLAIL* promotes the expression of the MYB family  
209 transcription factor *CIR1*, which in turn broadly contributes to gene expression. This may also explain  
210 why some genes are *FLAIL*-regulated but lack chromatin interactions with *FLAIL*. *CIR1* is a circadian  
211 clock gene, induced by light and involved in a regulatory feedback loop that controls a subset of the  
212 circadian outputs [52]. Our GO analysis supports that a subset of DEGs are connected to the  
213 response to red or far red light that contains among other key flowering genes such as  
214 *PHYTOCHROME INTERACTING FACTOR 4* (*PIF4*) and *CONSTANS* (*CO*) (Fig. S10B). *FLAIL* also  
215 binds the chromatin region of *LAC8*. *LAC8* is a laccase family member that mainly modulates  
216 phenylpropanoid pathway for lignin biosynthesis [53, 58]. Similar to *flail*, *lac8* mutants flower early [53].  
217 While intermediates in this pathway [59, 60] or dysregulation of lignin-related genes [21, 22, 61] could  
218 promote flowering in plants, the molecular connections of reduced *LAC8* expression to effects on  
219 flowering time will require further investigation. Nevertheless, our observations of reduced expression

220 of *LAC8* and *CIR1* in *flail*, combined with restored expression upon re-introduction of *FLAIL*, and direct  
221 *FLAIL* binding to *LAC8* and *CIR1* chromatin, suggested that early flowering in *flail* may result from  
222 combined direct and indirect effects of *LAC8* and *CIR1* repression.  
223 The range of plausible candidate mechanisms by which *FLAIL* may promote gene expression includes  
224 targeting of chromatin modifying complexes to activate gene expression as shown for the mammalian  
225 lncRNA *HOTTIP* [62], or effects on pre-mRNA RNA processing to stimulate mRNA expression as  
226 indicated for the plant lncRNA *ASCO* [63-65]. While our results clarify key aspects of functional units  
227 of the non-coding genome, it will remain an exciting future research endeavor to elucidate how sense  
228 *FLAIL* mediates the activation of floral repressor genes at the molecular level.  
229

### 230 **Identification of the functional *FLAIL* RNA isoform of the *FLAIL* locus**

231 A challenge in the field of lncRNA biology is the functional characterization of lncRNA loci. Our  
232 functional dissection of *FLAIL* illustrates these challenges, yet reveals a compelling example for a  
233 *trans*-acting lncRNA. Like many other loci, *FLAIL* generates multiple transcript isoforms, including  
234 cryptic transcript isoforms that would be missed by most standard transcriptomic approaches. DNA  
235 regulatory elements embedded in lncRNA loci and the act of lncRNA transcription may regulate the  
236 expression of neighboring genes (*cis*-acting) [66, 67]. However, disruption of the *FLAIL* locus had no  
237 significant impact on gene expression in a surrounding ~150 kb genomic window (from upstream  
238 AT2G18560 to downstream AT2G18940). These observations argue against the hypothesis that the  
239 *FLAIL* locus acts as a *cis*-acting RNA or DNA element. In contrast, we found genetic evidence that  
240 the *FLAIL* sense lncRNA functions as a *trans*-acting RNA. First, exogenous expression of *FLAIL*  
241 sense RNA *in vivo* rescues the early flowering phenotype as well as the expression of flowering genes  
242 in *flail3*. The rescue is specific for the *FLAIL* lncRNA encoded by the sense strand. Second, amiRNA  
243 mutants that specifically knock-down *FLAIL* sense RNA levels without effect on the DNA also show  
244 early flowering. Collectively, these data indicate that the role of the *FLAIL* locus in the repression of  
245 flowering is executed by a *trans*-acting lncRNA derived from the sense strand.

246 We assessed the protein-coding potential of *FLAIL* using a series of software tools that give low  
247 scores, arguing against a protein encoded by *FLAIL*. Nevertheless, Ribo-seq identifies ribosome  
248 association of *FLAIL*, consistent with two small ORFs with ~9 amino acids (Fig. S1B) [39]. Even  
249 though we found no evidence for peptide production in proteomics data, sORFs embedded in  
250 lncRNAs may encode for functional peptides [68, 69]. In our allelic series of *flail* mutants only *flail1*  
251 mutates the potential sORFs, while *flail2* and *flail3* keep the DNA sequences encoding the potential  
252 sORFs intact. The range of genetic mutations thus argue against the contribution of potential sORFs  
253 peptides to flowering, since the early flowering phenotype is similar in all three mutant backgrounds.  
254 Moreover, the microhomology with *Camelina* mapped to the 3'-region of *FLAIL* where we identified  
255 no ribosome association. While future experimental research in *Camelina sativa* would be needed to

256 examine functional conservation in flowering, the microhomology of *FLAIL* in other Brassicaceae is  
257 consistent with functional RNA domains that are a characteristic of conserved *trans*-acting lncRNAs.

258

## 259 **Conclusions**

260 In summary, this work highlights the contribution of lncRNAs to fine tune the complex developmental  
261 transition to initiate flowering. Regulation for key developmental decisions by lncRNA-based  
262 mechanisms may confer specific organismal advantages, yet detecting the functional roles of the non-  
263 coding genome may also be facilitated in the developmental context. RNA-based regulation of plant  
264 reproductive development through *trans*-acting lncRNA promises future possibilities for plant breeding  
265 research to improve Brassicaceae crop quality and resilience.

266

## 267 **Methods**

### 268 **Plant materials and growth conditions**

269 Table S8 provides a complete overview of the plant materials used in this study. Seeds of *flail3*  
270 (SMA2648, Table S8) were obtained from the Nottingham *Arabidopsis* Stock Centre and genotyping  
271 was performed using primers Mlo37/1788/1789 (Additional file 2 Table S9). *A. thaliana* plants were  
272 grown in a growth chamber with a long day photoperiod (16-h light/8-h dark) at 20 °C at a photo flux  
273 density of approximately 100 μmol/m<sup>2</sup>/sec in the chamber. For seedling treatments, seeds were  
274 surface-sterilized and placed on ½ MS + 1% sucrose plates at 4 °C in darkness for 3 days prior to  
275 germination. Then, plates were placed in the growth chamber in control conditions at 20 °C and  
276 sampled.

277

### 278 **CRISPR/Cas9-directed *flail* mutants**

279 Construction of a dual sgRNA-directed *flail1* (*goi*, [44]) knockout SMA3677 (Table S8) was performed  
280 by CRISPR/Cas9 using the described protocol [44]. Similarly, to generate the CRISPR mutant *flail2*  
281 (SMA3678, Table S8), plasmid pHEE2E-TRI (SMC528) harboring two sets of gBlocks including  
282 gBlock1 (a U6-26 promoter, a 19 bp target sequence 1, a sgRNA scaffold, a terminator) and gBlock2  
283 (a U6-29 promoter, a 19 bp target sequence 2, a sgRNA scaffold, a terminator) served as a template  
284 to amplify the middle border (Bsal-overhang1-protospacer1-scaffold-terminator-U6-29 promoter-  
285 protospacer2-overhang2-Bsal) using primer pairs Mlo1757 & Mlo1758 (Table S9). Second, both  
286 pKIR1.1 plasmid (SMC529) and the middle border were digested by AarI and Bsal, respectively, then  
287 the middle border was integrated into the linearized pKIR1.1 backbone to generate pKIR1.1-dual-  
288 sgRNA2 SMC575 (Table S10) for plant transformation. Third, after transformation using  
289 *Agrobacterium tumefaciens* strain SMA111 (Table S11), the T1 generation plants for successful T-  
290 DNA insertion events were selected by identifying seeds with red fluorescence, then seeds from  
291 individual T1-genotyped plants were harvested and grown. Finally, T2 mutants that did not contain

292 the CRISPR/Cas9 construct were identified by picking up T2 seeds without red fluorescence. PCR  
293 products were amplified from Cas9-free T2 plants using oligonucleotides Mlo2478/2479 (Table S9)  
294 flanking the deletion site for Sanger sequencing.

295

## 296 **Complementation assay**

297 Complementation constructs were generated using SMC431. *pFLAIL:FLAIL* and *pasFLAIL:asFLAIL*  
298 were amplified from genomic wild type DNA using primers MLO1746/1747 and MLO1759/1761,  
299 respectively (Table S9). The resulting PCR products were inserted into pENTR-D-Topo by topo  
300 cloning to generate entry vectors SMC542 and SMC541 (Table S10). The entry vectors were used in  
301 a LR reaction with SMC431 to generate expression vector SMC546 (containing *pFLAIL:gFLAIL*  
302 construct) and SMC545 (containing *pasFLAIL:gasFLAIL* construct) (Table S10). The  
303 complementation constructs together with the control vector *35S:GUS* (SMC377) were then  
304 transformed into GV3101 to get strains SMA112-114 (Table S11), followed by transformation into the  
305 *flail3* mutant. Seeds from transformed *Arabidopsis* plants were screened for T-DNA integration by  
306 hygromycin resistance. Multiple independent single-locus insertions were identified by segregation  
307 analysis and homozygous T3 transgenic plants SMA4477 for *flail3* *35S:GUS*, SMA4462 for *flail3*  
308 *pFLAIL:gFLAIL18*, SMA4464 for *flail3* *pFLAIL:gFLAIL88*, SMA4467 for *flail3* *pasFLAIL:gasFLAIL18*,  
309 SMA4468 for *flail3* *pasFLAIL:gasFLAIL39* were used for the complementation assay (Table S8).

310

## 311 **Cloning of amiRNA**

312 To construct *amiR-FLAILs*, we designed two artificial miRNA sequences in the miR319a backbone  
313 using Web MicroRNA Designer (WMD3) software to generate four oligonucleotide sequences (I to IV)  
314 (Mlo1774-1781, Table S9), which were used to engineer the amiRNA into the endogenous miR319a  
315 precursor by site-directed mutagenesis. The amiRNA containing precursor was generated by  
316 overlapping PCR using SMC532 as a template following the protocol described in the WMD3  
317 publication [46]. The fragment containing the amiRNA sequence was then introduced into pENTR-D-  
318 Topo by topo cloning to generate entry vectors (SMC547 for *amiR-FLAIL11-Topo* and SMC548 for  
319 *amiR-FLAIL12-Topo*) (Table S10). The entry vectors were used in a LR reaction with SMC531 to  
320 generate expression vector SMC558 (containing *amiR-FLAIL11* construct) and SMC559 (containing  
321 *amiR-FLAIL12* construct). Plant transformation was performed using *Agrobacterium* strains SMA115-  
322 117 (Table S11). Finally, homozygous T3 transgenic plants SMA4469, SMA4471, and SMA4480  
323 (Table S8) were used in this study.

324

## 325 **Gene expression analysis by PCR/RT-(q)PCR**

326 For the comparative expression analysis with *C. sativa*, genomic DNA was extracted from wild type  
327 *A. thaliana* and *C. sativa* seedlings (~1.5 weeks) and mature leaves (~4 weeks) using the DNeasy  
328 Plant Mini kit (Qiagen #69104) and diluted to 5 ng/μl. Total RNA was extracted from the same tissues

329 using the RNeasy Plant Mini kit (Qiagen #74904) with RNase-free DNase set (Qiagen #79254).  
330 Reverse transcription (RT) was performed on 1 µg of DNase-treated total RNA using the iScript cDNA  
331 synthesis kit (Bio-Rad #1708890), with the same amount of total RNA diluted in water as negative  
332 controls for RT-PCR. Primers (Table S9) were designed to amplify *AthaFLAIL* (AT2G18735),  
333 *CsatFLAIL-like* (*C. sativa*, Ensembl v51 Chr17 3432317-3432814), and *GAPDH* as an amplification  
334 control. Two reverse primers were designed to target different portions of *AthaFLAIL* and *CsatFLAIL-*  
335 *like*. The *GAPDH* primers amplify both *AthaGAPDH* and *CsatGAPDH*. PCR was performed with  
336 templates consisting of either 20 ng of genomic DNA, 50 ng of total RNA, or 50 ng of total RNA that  
337 had been reverse transcribed. 35 cycles of amplification were performed for all template types. PCR  
338 products were visualized after agarose gel electrophoresis using the Bio-Rad Chemi-doc imaging  
339 platform.

340 For reverse transcription quantitative real-time PCR, total RNA was extracted from two-week old  
341 *Arabidopsis* seedlings using an RNeasy Plant Mini Kit (Qiagen, Germany). DNA in the isolated RNA  
342 were digested with TURBO DNase (Thermo Fisher Scientific, USA). Purified RNA was subsequently  
343 reverse transcribed into cDNA with iScript™ cDNA Synthesis Kit (Bio-Rad, USA) following  
344 manufacturer's instructions. For real-time PCR analysis, the resulting cDNA was diluted ten-fold and  
345 used as a template in a PCR reaction with GoTaq qPCR Master mix (Promega, USA) and run on a  
346 CFX384 Touch instrument (Bio-Rad, USA) with an initial denaturation at 95 °C for 2 minutes, followed  
347 by 40 cycles at 95 °C for 15 seconds, 60 °C for 1 minute. Primer efficiencies were evaluated on a  
348 standard curve generated using a 10-fold dilution series of the sample over four dilution points.  
349 Relative expression was calculated and normalized to the internal reference gene *UBQ*. All primers  
350 (Table S9) did not show any evidence for non-specific products in the melting curve analysis.

351

### 352 **Chromatin isolation by RNA purification (ChIRP)**

353 ChIRP was performed as previously described with some modifications [70]. Probe design: The  
354 antisense oligonucleotide probes were designed against the full-length *FLAIL* sequence using the  
355 online probe designer at [www.singlemoleculefish.com](http://www.singlemoleculefish.com) [71]. The probes were biotinylated at the 3' end.  
356 To assess the specificity of the target capture by the oligonucleotides, the *FLAIL* probes were divided  
357 into two pools, Odd (Mlo2885) and Even (Mlo2886). All the experiments were carried out using both  
358 pools independently. Sixteen biotinylated oligonucleotide probes complementary to the *LUCIFERASE*  
359 transcript were pooled (Mlo2887) as negative control (Table S9).

360 RNA immunoprecipitation: Two-week old seedlings were crosslinked in 3% formaldehyde solution by  
361 vacuum infiltration for 25 minutes and then quenched by the addition of 0.125 M glycine at room  
362 temperature for 5 minutes. After washing and drying, crosslinked seedlings (2.5 g) were ground to a  
363 fine power in liquid nitrogen and suspended in 10 ml Honda Buffer (0.44 M Sucrose, 1.25% Ficoll,  
364 2.5% Dextran T40, 20 mM Hepes KOH with pH 7.4, 10 mM MgCl<sub>2</sub>, 0.5% Triton X-100, 5 mM DTT, 1

365 mM PMSF, 1 × Cocktail, and 2 U/ml RNase inhibitor). The samples were put on ice and mixed gently  
366 at 4 °C until the solution became homogenous, then filtered through two layers of Miracloth,  
367 centrifuged at 4000 rpm for 15 minutes at 4 °C. Pellets were resuspended in 1.5 ml Honda buffer and  
368 centrifuged at 4000 rpm for 15 minutes at 4 °C. Resuspending and centrifugation were repeated until  
369 the pellet was no longer green, typically two more times (~15 minutes). Pellets were suspended in  
370 1600 µl nuclear lysis buffer (50 mM Tris-HCl, pH 7.5, 2 mM MgCl<sub>2</sub>, 1% SDS, 0.1 mM PMSF, 10 mM  
371 EDTA, 1 mM DTT, 1 × Cocktail, 0.1 U/µl RNase Inhibitor) and sonicated at M setting 5 minutes (30  
372 seconds on and 30 seconds off) × 3 times by sonicator (QSONICA Q700, USA) until DNA was  
373 fragmented into 200–500 bp pieces. After centrifugation at 12,000 g at 4 °C for 10 minutes, the  
374 supernatant (around 1.5 ml) was diluted with 2 volumes of pre-heated hybridization buffer (750 mM  
375 NaCl, 1% SDS, 50 mM Tris, pH 7.5, 1 mM EDTA, 15% formamide, and 1 × protease inhibitor). The  
376 clear mixture was divided into 4 equal aliquots (IP-RNA and IP-DNA for both Even and Odd probes).  
377 Biotinylated DNA probe (2 µl of 100 pmol/µl) was added to each aliquot and incubated at 37 °C for 4  
378 hours with gentle mixing. Then 50 µl of well-washed Streptavidin C1 magnetic beads were added to  
379 each sample and incubated at 37 °C for 30 minutes. Captured beads were washed three times with  
380 high salt wash buffer (2 × SSC, 0.5% SDS, 1 mM DTT, and 1 mM PMSF) and three times with low  
381 salt wash buffer (0.1 × SSC, 0.5% SDS, 1 mM DTT, and 1 mM PMSF).  
382 RNA isolation: Beads were resuspended in 200 µl RNA elution buffer (100 mM NaCl, 50 mM Tris-HCl  
383 with pH 7.5, 1 mM EDTA, 1% SDS) and boiled for 15 minutes. RNA samples were treated with  
384 Proteinase K (1 mg/ml) at 65 °C for 1 h while shaking. RNA was extracted using TRIzol method, and  
385 then treated with DNase (Qiagen). RNA was used for RT-qPCR analysis to confirm RNA retrieval.  
386 DNA isolation: DNA was eluted with elution buffer (200 mM NaCl, 50 mM NaHCO<sub>3</sub>, 1% SDS, 10%  
387 SDS, 0.1 U/µl RNase H). After Proteinase K treatment at 45 °C for 1 h, DNA was extracted using ChIP  
388 DNA Clean & Concentrator (Zymo Research) and used for subsequent qPCR analysis or high-  
389 throughput sequencing.  
390

### 391 **Comparative Genomics:**

392 FLAIL sequence similarities were initially identified through reciprocal best BLAST against eleven  
393 disparate Brassicaceae genomes in CoGe BLAST [72] with an e-value of 10<sup>-5</sup>. As no hits were  
394 identified in a species more distantly related than *Camelina sativa*, comparative analysis was  
395 restricted to *Arabidopsis* and *Camelina*. Genomic regions displaying sequence similarity to the  
396 *Arabidopsis* *FLAIL* locus in the *Arabidopsis thaliana* (TAIR10) and *Camelina sativa* (Ensembl v2.0)  
397 were identified using CoGe BLAST, with regions of microsynteny identified using GEvo [73].  
398 Nucleotide sequence for syntenic regions were extracted and imported into Geneious Prime  
399 v2021.2.2 [74]. Multiple sequence alignments were used to design primers that specifically amplified  
400 a portion of *FLAIL* and the *FLAIL-like* intergenic region in *Camelina*.

402 **Statistical analysis**

403 The number of rosette leaves were measured with ImageJ software [75]. Statistical analysis was  
404 performed using the R software [76] or GraphPad Prism 9 [77]. For comparisons, data were evaluated  
405 using Student's t-test for significance of differences: \* means  $p$  value < 0.05, \*\* means  $p$  value < 0.01.

406

407 **Bioinformatics**

408 All the supporting code for bioinformatics analysis is repository available at FLAIL\_2021 from GitHub  
409 (<https://github.com/Yu-Jin-KU>) [78].

410

411 **Sequencing analysis**

412 RNA-seq libraries were prepared using NEXTFLEX® Rapid Directional RNA-seq Library Prep Kit  
413 (NOVA-5138-08) and ChIP-seq libraries were constructed using the ChIP-seq Library Prep Kit  
414 (NOVA-5143-02 with NEXTflex® ChIP-seq Barcodes-24) following the manufacturer's protocol and  
415 quantified on Agilent 2100 Bioanalyzer. Both RNA-seq and ChIP-seq libraries were pooled into one  
416 flow cell (NextSeq 500/550 High Output Kit v2.5) for sequencing in PE mode (2\*75 bp) on Illumina  
417 Nextseq 500.

418 Previously published RNA-seq datasets for wild type and PCP (SME1) deficient plants were  
419 downloaded from European Nucleotide Archive (accession number PRJEB24412) and from Gene  
420 Expression Omnibus (accession number GSE116964). The raw reads were quality controlled by the  
421 FastQC software [79], adapter trimmed by Trimmomatic v0.39 [80] in paired-end mode and then  
422 aligned to TAIR10 genome assembly by STAR v2.7.8a [81] in Local mode. Aligned reads with MAPQ  
423 below 10 were removed by Samtools v1.1.2 [82]. BAM files were converted to unstranded Bedgraph  
424 files using BEDtools genomecov v2.30.0 [78]. The code was detailed in the RNA-seq.sh script on the  
425 GitHub page mentioned above. Differentially expressed genes (DEGs) were called using the DESeq2  
426 tool [83]. Expression fold change values were log2 transformed to identify genes with statistically  
427 significant differential expression using the following criteria:  $|\log_2 \text{fold change}| > 1$  and adjusted  $p$   
428 value < 0.05. GO enrichment analysis was done by Metascape [47].

429 ChIP-seq reads were quality controlled by the FastQC software [79], adapter trimmed using Trim  
430 Galore v0.6.7 [84] and mapped to the TAIR10 genome using STAR v2.7.8a [81]. The converted BAM  
431 files were sorted and filtered for  $\text{MAPQ} \geq 5$ . After removing PCR duplicates by Samtools v1.1.2 [82],  
432 peaks of *FLAIL* occupancy were called with CCAT3.0 [48]. By using CHIPseeker [85] and  
433 TxDb.Athaliana.BioMart.plantsmart28 [86] packages in R, peak annotation was performed with the  
434 definition for a promoter being 300 bp around the TSS. Alignment statistics were provided in Table  
435 S3. Visualization and analysis of genome-wide enrichment profiles were done with IGV genome  
436 browser [87].

437

438 **Abbreviations**

439 amiRNAs: artificial microRNAs  
440 ChIRP: chromatin isolation by RNA purification;  
441 CIR1: CIRCADIAN 1;  
442 CNIT: Coding-NonCoding Identifying Tool;  
443 CO: CONSTANS;  
444 CPC2: Coding Potential Calculator;  
445 DEGs: differentially expressed genes;  
446 FLAIL: flowering associated intergenic lncRNA;  
447 FLC: FLOWERING LOCUS C;  
448 LAC8: LACCASE 8;  
449 lncRNAs: long non-coding RNAs;  
450 LUC: Luciferase;  
451 NMT3: PHOSPHOETHANOLAMINE N-METHYLTRANSFERASE 3;  
452 sORFs: small open reading frames;  
453 PCP: PORCUPINE;  
454 PIF4: PHYTOCHROME INTERACTING FACTOR 4  
455 plaNET-seq: plant Native Elongating Transcripts sequencing  
456 PLL25: PECTIN LYASE-LIKE 25;  
457 RNAPII: RNA polymerase II;  
458 SAMs: shoot apical meristems;  
459 SME: Sm protein E1;  
460 TIF-seq: Transcript Isoform sequencing;  
461 TSS-seq: Transcription Start Site sequencing;  
462 UBQ: UBIQUITIN  
463 WMD: Web MicroRNA Designer  
464

465 **Figure legends**

466  
467 **Fig. 1** Phenotypes of *FLAIL* knock-down plants. **A** Genome browser screenshot of plaNET-seq, TSS-  
468 seq and TIF-seq at the *FLAIL* genomic region in Col-0 and *hen2-2* mutant. Sense (+) and antisense  
469 (-) strands were shown in red and dark blue, respectively. Grey bar and light blue bar indicated primer  
470 locations of RT-qPCR for sense *FLAIL* (*FLAIL*) and antisense *FLAIL* (*asFLAIL*), respectively. **B**  
471 Coding potential of the transcript in the genomic region of *FLAIL* and *asFLAIL* and reference  
472 transcripts including non-coding RNAs (*18sRNA*, *U6*, *ELENA1*, *SVALKA*) and coding gene *UBQ*  
473 according to the CNIT and CPC2 algorithm. **C-D** Detection of *FLAIL* and *asFLAIL* gene expression in

474 Col-0 and *flail* mutants by RT-qPCR. Transcript levels were normalized to *UBQ* expression levels. Y-  
475 axis showed relative values compared to the expression level of Col-0. Bars represented average  $\pm$   
476 s.e.m (n = 3 independent 14-d seedling pools). \*, p value < 0.05 and \*\*, p value < 0.01 by Student's  
477 t-test compared to Col-0. **E** Morphological phenotypes of 4-week-old plants of Col-0, *flail* mutants at  
478 20 °C under a 16-h light/8-h dark growth condition. Scale bar: 2 cm. **F** Violin graph showed number  
479 of rosette leaves after appearance of the first flower bud in Col-0. Data represented the mean of six  
480 independent experiments. Boxes spanned the first to third quartile, bold black lines indicated median  
481 value for each group and whiskers represented the minimum and maximum values. \*, p value < 0.05  
482 was indicated by Student's t-test compared to Col-0.

483

484 **Fig. 2** *Sense-FLAIL* RNA is functional for flowering. **A** Schematic representations of the T-DNA  
485 constructs containing the native promoter of *sense-FLAIL* (native-Pro) fused to the *sense-FLAIL* DNA  
486 region with NOS as a terminator or the native promoter of *anti-sense FLAIL* (anti-native-Pro) fused to  
487 the *anti-sense FLAIL* DNA region or a negative control with the 35S promoter (35S) fused to GUS  
488 reporter were transformed into *flail3* *Arabidopsis* plants. **B-C** Detection of *FLAIL* and *asFLAIL* genes  
489 expression in Col-0, *flail3* mutant and complemented lines expressing *pFLAIL:gFLAIL* and  
490 *pasFLAIL:gasFLAIL* by RT-qPCR. Transcript levels were normalized to *UBQ* expression levels. Y-  
491 axis showed relative values compared to the expression level of Col-0. Error bars represented s.e.m  
492 (n = 3 independent 14-d seedling pools). \*, p value < 0.05 and \*\*, p value < 0.01 by Student's t-test  
493 compared to Col-0. **D** Representative morphological phenotypes of 4-week-old plants of Col-0, *flail3*  
494 mutant, transgenic lines at 20 °C under a 16-h light/8-h dark growth condition. Scale bar: 2 cm. **E**  
495 Violin graph showed number of rosette leaves after appearance of the first flower bud in Col-0. Data  
496 represented the mean of six independent experiments. Boxes spanned the first to third quartile, bold  
497 black lines indicated median value for each group and whiskers represented the minimum and  
498 maximum values. \*, p value < 0.05 was indicated by Student's t-test compared to Col-0.

499

500 **Fig. 3** *FLAIL* regulates flowering related genes. **A** Heatmap and hierarchical clustering of top 70  
501 differentially expressed genes (DEGs) in *flail3* versus Col-0 that were best rescued in the *flail3*  
502 *pFLAIL:gFLAIL18* complementation line. DEGs analyzed by DESeq2 with  $|\log_2 \text{fold change}| > 1$  and  
503 adjusted p value < 0.05 were considered significant differential expression. Three biological replicates  
504 for *flail3*, wild type, and two for *flail3 pFLAIL:gFLAIL18*. Flowering genes were highlighted in yellow  
505 bold. Samples clustered together on the basis of corresponding similar expression profiles. The color  
506 scale reflected the log 2-fold change in gene expression, ranging from down-regulated (blue) to up-  
507 regulated (red). **B-E** Genome browser screenshots illustrating the expression of dysregulated  
508 flowering genes in *flail3* were rescued in complementation line (top panel). Normalized read counts  
509 (TPM from RNA-seq) for differentially expressed flowering genes in WT, *flail3*, and *flail3*  
510 *pFLAIL:gFLAIL18* plants (bottom panel). Boxes spanned the first to third quartile, bold black lines

511 indicated median value for each group and whiskers represented the minimum and maximum values.  
512 All *p* values were denoted by Students' t-test. Bar = 500 bp.

513  
514 **Fig. 4** *FLAIL* affects flowering by chromatin binding of flowering genes. **A** Top, *FLAIL* bound the locus  
515 itself by ChIRP-seq from two independent Odd and Even probed chromatin. Luc probe was used as  
516 a control. Bottom, schematic representation of the antisense oligonucleotide probes that were  
517 biotinylated at the 3'-end with Odd (in red) and Even (in dark blue) against *FLAIL* sense RNA and Luc  
518 probe (in grey) against *LUC* mRNA. **B** ChIRP-qPCR using probe pools *FLAIL*-asDNA (Odd and Even)  
519 retrieved ~5%–10% of *FLAIL* endogenous RNA and < 1% levels of *UBQ*. *Luc*-asDNA probes  
520 retrieved much lower levels of both RNAs as a control. **C** *FLAIL* DNA signal was identified in both  
521 Odd and Even probes. *UBQ* region showed much less binding signal in all probes as a negative  
522 control. Graphs in **B** & **C** showed the mean ± s.e.m. (n= 3 independent replicates). **D**, **G** Genome  
523 browser screenshots illustrating two of *FLAIL* bound targets *CIR1* (**D**) and *LAC8* (**G**) in RNA-seq (lane  
524 1-3) and ChIRP-seq (lane 4-6). *FLAIL* binding peaks were called by CCAT3.0 with the cutoff FDR =  
525 0.232. **E**, **H** Normalized read counts (TPM from RNA-seq) for differentially expressed (DE) flowering  
526 genes in WT, *flail3*, and *flail3 pFLAIL:gFLAIL18* plants (bottom panel). Boxes spanned the first to third  
527 quartile, bold black lines indicated median value for each group and whiskers represented the  
528 minimum and maximum values. **F** Venn diagram of genes targeted by *FLAIL* (ChIRP-seq) and genes  
529 overlapped with DEGs in *flail3* and flowering related genes. **I** A model for the *trans*-acting *FLAIL* sense  
530 RNA regulated flowering. The *FLAIL* sense RNA binds chromatin regions of flowering genes to  
531 regulate expression levels of flowering related genes and thus affects flowering time. All *p* values  
532 were denoted by Students' t-test.

533  
534 **Supplementary information**  
535 **Fig. S1** Characterization of *FLAIL* locus. **A** Genome browser view of *FLAIL* splicing status in nanopore  
536 sequencing of Col-0. Transcription of sense *FLAIL* RNA and *asFLAIL* RNA were shown in red and  
537 dark blue, respectively and no isoform resulting from alternative splicing was observed. **B** *FLAIL*  
538 nucleotide sequences in black and two sORFs locations in blue.

539  
540 **Fig. S2** Assessment of *FLAIL* and *UBQ* for protein coding potential. Initiation codon translational  
541 analysis using NetStart for *FLAIL* and *UBQ*. The predicted initiation codons were depicted with the  
542 letter i, other instances of "ATG" by the letter "N" (non-start). The dots (".") were place holders for all  
543 the other sequence elements. The scores were always in [0.0, 1.0]; when greater than 0.5, they  
544 represented a probable translation start.

545

546 **Fig. S3** Sequence and transcriptional conservation at the *FLAIL* and *FLAIL-like* loci in *Arabidopsis*  
547 and *Camelina*. **A** Schematic depicting the conservation of the *Arabidopsis* (*A.tha*) *FLAIL* locus in  
548 *Camelina sativa* (*C.sat*). Green boxes represent exons, with triangles representing direction of  
549 transcription. The *FLAIL* locus is represented by a yellow box. Faded blue lines represent sequence  
550 similarity between different loci. Dashed boxes at the *FLAIL* and *Csa17g011930* loci represent regions  
551 targeted for RT-PCR. **B** Amplification of *A.thaFLAIL* and *C.satFLAIL-like*, using RNA template (+/- RT,  
552 lanes 1-20). NT indicates no template was added to the reaction. **C** Control amplifications: *GAPDH*  
553 was amplified using RNA template (+/- RT, lanes 21-29), and *A.thaFLAIL* and *C.satFLAIL-like* were  
554 amplified using genomic DNA template (lanes 30-41). L indicates leaf tissue, S indicates seedling  
555 tissue.

556

557 **Fig. S4** *FLAIL* dual-sgRNA approach and T-DNA insertion genotyping. **A** Schematic representation  
558 of targeted gene *FLAIL* with locations of two Cas9-directed mutants *flail1*, *flail2*, and one T-DNA  
559 mutant *flail3*. Locations of dual-sgRNA target sites were shown in red arrow, primer pair F/R  
560 (Mlo2478/2479) were used for PCR testing deletion in *flail1* and *flail2*, triangle indicated the putative  
561 position of T-DNA insertion at the *FLAIL* locus. Blue boxes indicated two sORFs. **B** Similar to the  
562 previous generation of *flail1*, *FLAIL2* construct containing pKIR1.1 enabled red fluorescence selection  
563 of *flail2* seeds from T1 plants after transformation by floral dipping. **C** Genotyping of individual T1 plant  
564 with red fluorescence, Leaf genomic DNA of T1 plants were PCR amplified. Expected size of PCR  
565 product for deletion was 343 bp in *flail2* line. *flail2-32* in red box was selected for next generation. **D**  
566 In T2 selection, the null mutant *flail2-32-93* without red fluorescence in seeds represented Cas9-free  
567 plants, indicated by red box in **E**. PAM was shown in blue, sgRNA protospacers were in red, and  
568 deleted bases were replaced by dots. **E** PCR analysis of T2 lines. The expected size of the wild-  
569 type *FLAIL* amplicon and the deletion size between Cas9 cut sites in *flail2-32-93* were indicated. This  
570 inherited Cas9-null segregation line was used for data analysis in Fig. 1. **F** Genotyping of the T-DNA  
571 insertion mutant *flail3*. Gel sample order (from left to right): lane 1, marker; lane 2, WT; lane 3, *flail3*,  
572 with primer set, Mlo1788 + Mlo1789 + Mlo37; Results clearly showed that *flail3* line was homozygous  
573 since WT was the only line giving WT band and *flail3* line gave the only T-DNA insertion band.

574

575 **Fig. S5** *FLAIL* lncRNA functions as a flowering repressor. **A** Sequences and structures of amiRNA  
576 duplexes and the target sites of *amiR-FLAILs* and *amiR-FLAIL\**s. Upper panel, schematic  
577 representation of transcribed sense *FLAIL* RNA. Lower panel, sequences of amiRNA duplexes,  
578 amiRNA (in red) target sites, and potential amiRNA\* (in blue) on cognate sense *FLAIL* (in black). **B**  
579 Gene expression of sense *FLAIL* in *amiR-FLAIL* plants by RT-qPCR. Transcript levels were  
580 normalized to *UBQ* expression levels. Two representative lines for amiRNA designed transgenic  
581 plants were selected. Y-axis showed relative values compared to the expression level of empty vector  
582 transformed plants. Grey bars depicted the relative positions of primers used for RT-qPCR analyses.

583 Transcript levels were normalized to *UBQ* expression levels. Error bars represented s.e.m (n = 3  
584 independent 14-day seedling pools). \*\*, *p* value < 0.01 analyzed by Student's t-test. **C** Morphological  
585 phenotypes of 4-week-old plants of Col-0 and two *amiR-FLAIL* plants under a 16-h light/8-h dark  
586 growth condition. Scale bar: 2 cm. **D** Violin graph showed number of rosette leaves after appearance  
587 of the first flower bud in Col-0. Data represented the mean of six independent experiments. Boxes  
588 spanned the first to third quartile, bold black lines indicated median value for each group and whiskers  
589 represented the minimum and maximum values. \*\*, *p* value < 0.01 was indicated by Student's t-test  
590 compared to Col-0.

591  
592 **Fig. S6** Genome-wide effects of *FLAIL* on gene expression by RNA-seq. **A** Venn diagram of flowering  
593 genes overlapped with upregulated and downregulated genes in the *flail3* mutant and with unchanged  
594 genes in the *flail3 pFLAIL:gFLAIL18* complementation plant. **B** Reproducibility of all genes shown in  
595 Fig. 3 from RNA-seq data was demonstrated by clustered heatmap of Pearson correlation coefficients  
596 over all independent replicates of RNA-seq in WT, *flail3* mutant, and *flail3 pFLAIL gFLAIL18* plants.  
597 Darker red denoted higher correlation and darker blue represented low reproducibility.

598  
599 **Fig. S7** *FLAIL* regulates flowering related genes in *trans*. **A-F** Genome browser screenshots  
600 illustrating the expression of dysregulated flowering genes in *flail3* were most fully rescued in  
601 complementation line. Normalized read counts (TPM from RNA-seq) were used for differentially  
602 expressed flowering genes in WT, *flail3*, and *flail3 pFLAIL:gFLAIL18* plants. Boxes spanned the first  
603 to third quartile, bold black lines indicated median value for each group and whiskers represented the  
604 minimum and maximum values. *p* value was denoted by Students' t-test.

605  
606 **Fig. S8** Strategy to identify genome-wide binding profile of *FLAIL* analyzed by ChIRP-seq. **A**  
607 Illustration of *FLAIL* peaks called by CCAT3.0. Only peaks that occurred at target genes from both  
608 Even and Odd probed DNA, but not from two or more independent experiments of Luc pools were  
609 considered significant enrichment (Example 1), peaks that only occurred from either Even or Odd  
610 pools were not considered *FLAIL* targets (Example 2 & 3). **B** A pie chart that was generated by  
611 ChIPseeker represented distribution of *FLAIL* bound regions in the genome. A total of 210 *FLAIL*  
612 bound regions were annotated according to the genomic distribution and *FLAIL* was enriched  
613 predominantly in promoter regions.

614  
615 **Fig. S9** *FLAIL* binds chromatin regions of flowering genes for gene regulation. **A, C** Genome browser  
616 screenshots illustrating two more *FLAIL* bound flowering targets *PLL25* and *NMT3* in RNA-seq (lane  
617 1-3) and ChIRP-seq (lane 4-6). Their expression that was downregulated in *flail3* (lane 1) can be  
618 partially or fully rescued in complementation line (lane 2). Both Odd and Even probes identified  
619 chromatin binding regions of *FLAIL* in two more flowering genes *NMT3* and *PLL25* compared to *Luc*

620 probes. *FLAIL* binding peaks were called by CCAT3.0. **B, D** Normalized read counts (TPM from RNA-  
621 seq) for differentially expressed (DE) flowering genes in WT, *flail3*, and *flail3 pFLAIL:gFLAIL18* plants  
622 (bottom panel). Boxes spanned the first to third quartile, bold black lines indicated median value for  
623 each group and whiskers represented the minimum and maximum values. *p* value was denoted by  
624 Students' t-test.

625  
626 **Fig. S10** *FLAIL* regulates flowering independent of *PCP*. **A, B** Venn diagram showing overlapping  
627 differentially expressed genes (up/down) sets between *flail3* and *pcp* (also called *sme1*) mutants. **C,**  
628 **D** GO analysis of the DEGs in RNA-seq data of *flail3* and *pcp /sme1* mutants. Y-axis indicated the  
629 GO categories including biological process (BP), cellular component (CC) and molecular function  
630 (MF); X-axis showed -Log10 *p* value with the cutoff 0.05. Highly enriched GO terms of dysregulated  
631 mRNAs analyzed by the Metascape with 5 top enrichment scores.

632  
633 **Table S1.** DEGs in *flail3* mutant  
634 **Table S2.** DEGs in *flail3 pFLAIL gFLAIL18* plants  
635 **Table S3.** *FLAIL* targets called by CCAT3.0  
636 **Table S4.** Overlapping genes between DEGs in *flail3* and *FLAIL* targets.  
637 **Table S5.** Gene Ontology of DEGs in *flail3*  
638 **Table S6.** Gene Ontology of DEGs in *pcp* (RNA-seq data from Capovilla et al with the ENA accession:  
639 PRJEB24412)  
640 **Table S7.** Gene Ontology of DEGs in *sme1* (RNA-seq data from Huertas et al with the GEO accession:  
641 GSE116964)  
642 **Table S8.** Seeds  
643 **Table S9.** Primer sequences  
644 **Table S10.** Plasmids  
645 **Table S11.** GV3101 strains

646  
647 **Declarations**

648  
649 **Ethics approval and consent to participate**  
650 Not applicable

651  
652 **Consent for publication**  
653 Not applicable

654  
655 **Availability of data and materials**

656 The RNA-seq and ChIRP-seq data were deposited at GEO with the number GSE186215 [88]. The  
657 reagents described in this study are available from the corresponding author.

658

### 659 **Competing interests**

660 The authors declare they have no competing interests.

661

### 662 **Funding**

663 S.M. acknowledges the funding from the Novo Nordisk Foundation (NNF15OC0014202,  
664 NNF19OC0057485), a Copenhagen Plant Science Centre Young Investigator Starting grant and  
665 EMBO YIP. This project receives support from the European Research Council (ERC) under the  
666 European Union's Horizon 2020 Research and Innovation Programme (StG2017-757411 to S.M.).  
667 A.D.L.N. would like to acknowledge funding from NSF-IOS 1758532 and NSF-IOS 2023310.

668

### 669 **Authors' contributions**

670 Y.J. and S.M. conceived the study. Y.J. performed most experimental work, A.N.D. and A.D.L.N  
671 contributed comparative genomics and expression analysis in S3. M.I. and Y.J. did the computational  
672 analysis. Y.J. and M.S. wrote the manuscript.

673

### 674 **Acknowledgements**

675 We thank Prof. Anders H. Lund and for kindly providing Luc probes. We thank Prof. Peter Brodersen  
676 for sharing amiRNA vectors. We thank Dr. Pan Zhu and Dr. Marta Montes for assistance with ChIRP,  
677 Prof. Egle Kudirkiene and Dr. Quentin Thomas for sequencing. We thank Jasmin Dilgen, Evangelia  
678 Lakita, Ida Damholt Richardt, Lei Li for technical assistance, Jan Høstrup for excellent plant care, Dr.  
679 Deyong Zhu and the members of Marquardt lab for discussions and manuscript feedback.

680

681 **References**

- 682 1. Osman S, Cramer P. Structural Biology of RNA Polymerase II Transcription: 20 Years On. *Annu Rev Cell*  
683 *Dev Bi.* 2020;36:1-34.
- 684 2. Kapranov P, Cheng J, Dike S, Nix DA, Duttagupta R, Willingham AT, Stadler PF, Hertel J, Hackermuller  
685 J, Hofacker IL, et al. RNA maps reveal new RNA classes and a possible function for pervasive  
686 transcription. *Science.* 2007;316:1484-1488.
- 687 3. Choi SW, Kim HW, Nam JW. The small peptide world in long noncoding RNAs. *Brief Bioinform.*  
688 2019;20:1853-1864.
- 689 4. Gil N, Ulitsky I. Regulation of gene expression by cis-acting long non-coding RNAs. *Nature Reviews*  
690 *Genetics.* 2020;21:102-117.
- 691 5. Goff LA, Rinn JL. Linking RNA biology to lncRNAs. *Genome Res.* 2015;25:1456-1465.
- 692 6. Ivanov M, Sandelin A, Marquardt S. TranscriptomeReconstructoR: data-driven annotation of complex  
693 transcriptomes. *Bmc Bioinformatics.* 2021;22:290.
- 694 7. Jin Y, Marquardt S. Winter fields antisense RNAs to kick off flowering. *Gene Dev.* 2021;35:785-786.
- 695 8. Zhao YS, Zhu P, Hepworth J, Bloomer R, Antoniou-Kourouoni RL, Doughty J, Heckmann A, Xu CY, Yang  
696 HC, Dean C. Natural temperature fluctuations promote COOLAIR regulation of FLC. *Gene Dev.*  
697 2021;35:888-898.
- 698 9. Gowthaman U, Garcia-Pichardo D, Jin Y, Schwarz I, Marquardt S. DNA Processing in the Context of  
699 Noncoding Transcription. *Trends Biochem Sci.* 2020;45:1009-1021.
- 700 10. Chen L, Zhu QH, Kaufmann K. Long non-coding RNAs in plants: emerging modulators of gene activity  
701 in development and stress responses. *Planta.* 2020;252:92.
- 702 11. Kopp F, Mendell JT. Functional Classification and Experimental Dissection of Long Noncoding RNAs.  
703 *Cell.* 2018;172:393-407.
- 704 12. Ariel F, Lucero L, Christ A, Mammarella MF, Jegu T, Veluchamy A, Mariappan K, Latrasse D, Blein T, Liu  
705 C, et al. R-Loop Mediated trans Action of the APOLO Long Noncoding RNA. *Mol Cell.* 2020;77:1055-  
706 1065.
- 707 13. Moison M, Pacheco JM, Lucero L, Fonouni-Farde C, Rodriguez-Melo J, Mansilla N, Christ A, Bazin J,  
708 Benhamed M, Ibanez F, et al. The lncRNA APOLO interacts with the transcription factor WRKY42 to  
709 trigger root hair cell expansion in response to cold. *Mol Plant.* 2021;14:937-948.
- 710 14. Mishra K, Kanduri C. Understanding Long Noncoding RNA and Chromatin Interactions: What We Know  
711 So Far. *Noncoding RNA.* 2019;5:54.
- 712 15. Fan YR, Yang JY, Mathioni SM, Yu JS, Shen JQ, Yang XF, Wang L, Zhang QH, Cai ZX, Xu CG, et al. PMS1T,  
713 producing phased small-interfering RNAs, regulates photoperiod-sensitive male sterility in rice. *P Natl  
714 Acad Sci USA.* 2016;113:15144-15149.

715 16. Ding JH, Lu Q, Ouyang YD, Mao HL, Zhang PB, Yao JL, Xu CG, Li XH, Xiao JH, Zhang QF. A long noncoding  
716 RNA regulates photoperiod-sensitive male sterility, an essential component of hybrid rice. *P Natl Acad  
717 Sci USA*. 2012;109:2654-2659.

718 17. Fang J, Zhang FT, Wang HR, Wang W, Zhao F, Li ZJ, Sun CH, Chen FM, Xu F, Chang SQ, et al. Ef-cd locus  
719 shortens rice maturity duration without yield penalty. *P Natl Acad Sci USA*. 2019;116:18717-18722.

720 18. Henriques R, Wang H, Liu J, Boix M, Huang LF, Chua NH. The antiphasic regulatory module comprising  
721 CDF5 and its antisense RNA FLORE links the circadian clock to photoperiodic flowering. *New Phytol*.  
722 2017;216:854-867.

723 19. Severing E, Faino L, Jamge S, Busscher M, Kuijer-Zhang Y, Bellinazzo F, Busscher-Lange J, Fernandez V,  
724 Angenent GC, Immink RGH, Pajoro A. *Arabidopsis thaliana* ambient temperature responsive lncRNAs.  
725 *Bmc Plant Biol*. 2018;18:145.

726 20. Zhao XY, Li JR, Lian B, Gu HQ, Li Y, Qi YJ. Global identification of *Arabidopsis* lncRNAs reveals the  
727 regulation of MAF4 by a natural antisense RNA. *Nat Commun*. 2018;9.

728 21. Shi Y, Zhang X, Xu ZY, Li L, Zhang C, Schlappi M, Xu ZQ. Influence of EARLI1-like genes on flowering time  
729 and lignin synthesis of *Arabidopsis thaliana*. *Plant Biology*. 2011;13:731-739.

730 22. Xu B, Sathitsuksanoh N, Tang YH, Udvardi MK, Zhang JY, Shen ZX, Balota M, Harich K, Zhang PYH, Zhao  
731 BY. Overexpression of AtLOV1 in Switchgrass Alters Plant Architecture, Lignin Content, and Flowering  
732 Time. *Plos One*. 2012;7: e47399.

733 23. Cho LH, Yoon J, An G. The control of flowering time by environmental factors. *Plant Journal*.  
734 2017;90:708-719.

735 24. Csorba T, Questa JI, Sun QW, Dean C. Antisense COOLAIR mediates the coordinated switching of  
736 chromatin states at FLC during vernalization. *P Natl Acad Sci USA*. 2014;111:16160-16165.

737 25. Liu FQ, Marquardt S, Lister C, Swiezewski S, Dean C. Targeted 3' Processing of Antisense Transcripts  
738 Triggers *Arabidopsis* FLC Chromatin Silencing. *Science*. 2010;327:94-97.

739 26. Swiezewski S, Liu FQ, Magusin A, Dean C. Cold-induced silencing by long antisense transcripts of an  
740 *Arabidopsis* Polycomb target. *Nature*. 2009;462:799-U122.

741 27. Shin JH, Chekanova JA. *Arabidopsis* RRP6L1 and RRP6L2 Function in FLOWERING LOCUS C Silencing via  
742 Regulation of Antisense RNA Synthesis. *PLoS genetics*. 2014;10:e1004612.

743 28. Poole RL. The TAIR database. *Methods Mol Biol*. 2007;406:179-212.

744 29. Gallart AP, Pulido AH, de Lagran IAM, Sanseverino W, Cigliano RA. GREENC: a Wiki-based database of  
745 plant lncRNAs. *Nucleic Acids Res*. 2016;44:D1161-D1166.

746 30. Jia JB, Long YP, Zhang H, Li ZW, Liu ZJ, Zhao Y, Lu DD, Jin XH, Deng X, Xia R, et al. Post-transcriptional  
747 splicing of nascent RNA contributes to widespread intron retention in plants. *Nat Plants*. 2020;6:780-  
748 788.

749 31. Kindgren P, Ivanov M, Marquardt S. Native elongation transcript sequencing reveals temperature  
750 dependent dynamics of nascent RNAPII transcription in Arabidopsis. *Nucleic Acids Res.* 2020;48:2332-  
751 2347.

752 32. Nielsen M, Ard R, Leng X, Ivanov M, Kindgren P, Pelechano V, Marquardt S. Transcription-driven  
753 chromatin repression of Intragenic transcription start sites. *PLoS genetics.* 2019;15:e1007969.

754 33. Thomas QA, Ard R, Liu JH, Li BN, Wang JW, Pelechano V, Marquardt S. Transcript isoform sequencing  
755 reveals widespread promoter-proximal transcriptional termination in Arabidopsis. *Nat Commun.*  
756 2020;11:2589.

757 34. Kang YJ, Yang DC, Kong L, Hou M, Meng YQ, Wei LP, Gao G. CPC2: a fast and accurate coding potential  
758 calculator based on sequence intrinsic features. *Nucleic Acids Res.* 2017;45:W12-W16.

759 35. Guo JC, Fang SS, Wu Y, Zhang JH, Chen Y, Liu J, Wu B, Wu JR, Li EM, Xu LY, et al. CNIT: a fast and  
760 accurate web tool for identifying protein-coding and long non-coding transcripts based on intrinsic  
761 sequence composition. *Nucleic Acids Res.* 2019;47:W516-W522.

762 36. Seo JS, Sun HX, Park BS, Huang CH, Yeh SD, Jung C, Chua NH. ELF18-INDUCED LONG-NONCODING RNA  
763 Associates with Mediator to Enhance Expression of Innate Immune Response Genes in Arabidopsis.  
764 *Plant Cell.* 2017;29:1024-1038.

765 37. Kindgren P, Ard R, Ivanov M, Marquardt S. Transcriptional read-through of the long non-coding RNA  
766 SVALKA governs plant cold acclimation. *Nat Commun.* 2018;9:4561.

767 38. Pedersen AG, Nielsen H. Neural network prediction of translation initiation sites in eukaryotes:  
768 Perspectives for EST and genome analysis. Fifth International Conference on Intelligent Systems for  
769 Molecular Biology, Proceedings. 1997:226-233.

770 39. Palos K, Dittrich AN, Yu LA, Brock JR, Wu L, Sokolowska E, Skirycz A, Hsu PD, Lyons E, Beilstein MA,  
771 Nelson ADL. Identification and Functional Annotation of Long Intergenic Non-coding RNAs in the  
772 Brassicaceae. *bioRxiv.* 2021; doi:10.1101/2021.09.17.460835.

773 40. Hsu PY, Calviello L, Wu HYL, Li FW, Rothfels CJ, Ohler U, Benfey PN. Super-resolution ribosome profiling  
774 reveals unannotated translation events in Arabidopsis. *P Natl Acad Sci USA.* 2016;113:E7126-E7135.

775 41. Nelson ADL, Forsythe ES, Devisetty UK, Clausen DS, Haug-Batzell AK, Meldrum AMR, Frank MR, Lyons  
776 E, Beilstein MA. A Genomic Analysis of Factors Driving lincRNA Diversification: Lessons from Plants.  
777 *G3-Genes Genom Genet.* 2016;6:2881-2891.

778 42. Ross CJ, Rom A, Spinrad A, Gelbard-Solodkin D, Degani N, Ulitsky I. Uncovering deeply conserved motif  
779 combinations in rapidly evolving noncoding sequences. *Genome biology.* 2021;22.

780 43. Beilstein MA, Nagalingum NS, Clements MD, Manchester SR, Mathews S. Dated molecular phylogenies  
781 indicate a Miocene origin for *Arabidopsis thaliana*. *P Natl Acad Sci USA.* 2010;107:18724-18728.

782 44. Jin Y, Marquardt S. Dual sgRNA-based Targeted Deletion of Large Genomic Regions and Isolation of  
783 Heritable Cas9-free Mutants in Arabidopsis. *Bio-Protocol*. 2020;10:e3796.

784 45. Fedak H, Palusinska M, Krzyczmonik K, Brzezniak L, Yatusevich R, Pietras Z, Kaczanowski S, Swiezewski  
785 S. Control of seed dormancy in Arabidopsis by a cis-acting noncoding antisense transcript. *P Natl Acad  
786 Sci USA*. 2016;113:E7846-E7855.

787 46. Schwab R, Ossowski S, Riester M, Warthmann N, Weigel D. Highly specific gene silencing by artificial  
788 microRNAs in Arabidopsis. *Plant Cell*. 2006;18:1121-1133.

789 47. Zhou YY, Zhou B, Pache L, Chang M, Khodabakhshi AH, Tanaseichuk O, Benner C, Chanda SK.  
790 Metascape provides a biologist-oriented resource for the analysis of systems-level datasets. *Nat  
791 Commun*. 2019;10:1523.

792 48. Xu H, Handoko L, Wei XL, Ye CP, Sheng JP, Wei CL, Lin F, Sung WK. A signal-noise model for significance  
793 analysis of ChIP-seq with negative control. *Bioinformatics*. 2010;26:1199-1204.

794 49. Chen W, Salari H, Taylor MC, Jost R, Berkowitz O, Barrow R, Qiu D, Branco R, Masle J. NMT1 and NMT3  
795 N-Methyltransferase Activity Is Critical to Lipid Homeostasis, Morphogenesis, and Reproduction. *Plant  
796 physiology*. 2018;177:1605-1628.

797 50. Lashbrook CC, Cai S. Cell wall remodeling in Arabidopsis stamen abscission zones: Temporal aspects  
798 of control inferred from transcriptional profiling. *Plant signaling & behavior*. 2008;3:733-736.

799 51. Sun LX, van Nocker S. Analysis of promoter activity of members of the PECTATE LYASE-LIKE (PLL) gene  
800 family in cell separation in Arabidopsis. *Bmc Plant Biol*. 2010;10:152.

801 52. Zhang X, Chen Y, Wang ZY, Chen Z, Gu H, Qu LJ. Constitutive expression of CIR1 (RVE2) affects several  
802 circadian-regulated processes and seed germination in Arabidopsis. *The Plant journal : for cell and  
803 molecular biology*. 2007;51:512-525.

804 53. Cai XN, Davis EJ, Ballif J, Liang MX, Bushman E, Haroldsen V, Torabinejad J, Wu YJ. Mutant identification  
805 and characterization of the laccase gene family in Arabidopsis. *J Exp Bot*. 2006;57:2563-2569.

806 54. Heo JB, Sung S. Vernalization-Mediated Epigenetic Silencing by a Long Intronic Noncoding RNA.  
807 *Science*. 2011;331:76-79.

808 55. Kim DH, Sung S. Vernalization-Triggered Intragenic Chromatin Loop Formation by Long Noncoding  
809 RNAs. *Dev Cell*. 2017;40:302-312.

810 56. Capovilla G, Delhomme N, Collani S, Shutava I, Bezrukov I, Symeonidi E, Amorim MD, Laubinger S,  
811 Schmid M. PORCUPINE regulates development in response to temperature through alternative  
812 splicing. *Nat Plants*. 2018;4:534-539.

813 57. Huertas R, Catala R, Jimenez-Gomez JM, Castellano MM, Crevillen P, Pineiro M, Jarillo JA, Salinas J.  
814 Arabidopsis SME1 Regulates Plant Development and Response to Abiotic Stress by Determining  
815 Spliceosome Activity Specificity. *Plant Cell*. 2019;31:537-554.

816 58. Wang CY, Zhang SC, Yu Y, Luo YC, Liu Q, Ju CL, Zhang YC, Qu LH, Lucas WJ, Wang XJ, Chen YQ. MiR397b  
817 regulates both lignin content and seed number in *Arabidopsis* via modulating a laccase involved in  
818 lignin biosynthesis. *Plant Biotechnol J.* 2014;12:1132-1142.

819 59. Nakanishi F, Kusumi T, Inoue Y, Fujii T. Dihydrokaempferol Glucoside from Cotyledons Promotes  
820 Flowering in *Pharbitis-Nil*. *Plant and Cell Physiology.* 1995;36:1303-1309.

821 60. Hatayama T, Takeno K. The metabolic pathway of salicylic acid rather than of chlorogenic acid is  
822 involved in the stress-induced flowering of *Pharbitis nil*. *J Plant Physiol.* 2003;160:461-467.

823 61. Wang Y, Luo XJ, Sun F, Hu JH, Zha XJ, Su W, Yang JS. Overexpressing lncRNA LAIR increases grain yield  
824 and regulates neighbouring gene cluster expression in rice. *Nat Commun.* 2018;9:3516.

825 62. Ghafouri-Fard S, Dashti S, Taheri M. The HOTTIP (HOXA transcript at the distal tip) lncRNA: Review of  
826 oncogenic roles in human. *Biomed Pharmacother.* 2020;127.

827 63. Rigo R, Bazin J, Romero-Barrios N, Moison M, Lucero L, Christ A, Benhamed M, Blein T, Huguet S,  
828 Charon C, et al. The *Arabidopsis* lncRNA ASCO modulates the transcriptome through interaction with  
829 splicing factors. *Embo Rep.* 2020;21:e48977.

830 64. Bardou F, Ariel F, Simpson CG, Romero-Barrios N, Laporte P, Balzergue S, Brown JWS, Crespi M. Long  
831 Noncoding RNA Modulates Alternative Splicing Regulators in *Arabidopsis*. *Dev Cell.* 2014;30:166-176.

832 65. Fonouni-Farde C, Ariel F, Crespi M. Plant Long Noncoding RNAs: New Players in the Field of Post-  
833 Transcriptional Regulations. *Non-Coding Rna.* 2021;7:12.

834 66. Groff AF, Sanchez-Gomez DB, Soruco MML, Gerhardinger C, Barutcu AR, Li E, Elcavage L, Plana O,  
835 Sanchez LV, Lee JC, et al. In vivo characterization of Linc-p21 reveals functional cis-regulatory DNA  
836 elements. *Cell Rep.* 2016;16:2178-2186.

837 67. Paralkar VR, Taborda CC, Huang P, Yao Y, Kossenkov AV, Prasad R, Luan J, Davies JOJ, Hughes JR,  
838 Hardison RC, et al. Unlinking an lncRNA from its associated cis element. *Mol Cell.* 2016;62:104-110.

839 68. Chen J, Brunner AD, Cogan JZ, Nunez JK, Fields AP, Adamson B, Itzhak DN, Li JY, Mann M, Leonetti MD,  
840 Weissman JS. Pervasive functional translation of noncanonical human open reading frames. *Science.*  
841 2020;367:1140-1146.

842 69. Lewandowski JP, Dumbovic G, Watson AR, Hwang T, Jacobs-Palmer E, Chang N, Much C, Turner KM,  
843 Kirby C, Rubinstein ND, et al. The Tug1 lncRNA locus is essential for male fertility. *Genome biology.*  
844 2020;21:237.

845 70. Chu C, Quinn J, Chang HY. Chromatin isolation by RNA purification (ChIRP). *Journal of visualized  
846 experiments : JoVE.* 2012.

847 71. Raj A, van den Bogaard P, Rifkin SA, van Oudenaarden A, Tyagi S. Imaging individual mRNA molecules  
848 using multiple singly labeled probes. *Nat Methods.* 2008;5:877-879.

849 72. Nelson ADL, Haug-Baltzell AK, Davey S, Gregory BD, Lyons E. EPIC-CoGe: managing and analyzing  
850 genomic data. *Bioinformatics*. 2018;34:2651-2653.

851 73. Lyons E, Freeling M. How to usefully compare homologous plant genes and chromosomes as DNA  
852 sequences. *Plant Journal*. 2008;53:661-673.

853 74. Geneious Prime. <https://www.geneious.com>. Accessed 2021.

854 75. Schneider CA, Rasband WS, Eliceiri KW. NIH Image to ImageJ: 25 years of image analysis. *Nat Methods*.  
855 2012;9:671-675.

856 76. R Core Team. R: A language and environment for statistical computing. R Foundation for statistical  
857 computing, Vienna, Austria. <https://www.R-project.org/>. accessed.

858 77. GraphPad Prism 9. GraphPad Software, Inc. <http://www.graphpad.com> Accessed 1 Jan 2021

859 78. Jin Y. FLAIL\_2021. <https://github.com/Yu-Jin-KU>. Accessed 12 Aug 2021.

860 79. Andrews S. FastQC: a quality control tool for high throughput sequence data.  
<http://www.bioinformatics.babraham.ac.uk/projects/fastqc>. Accessed 18 Jan 2019.

861 80. Bolger AM, Lohse M, Usadel B. Trimmomatic: a flexible trimmer for Illumina sequence data.  
*Bioinformatics*. 2014;30:2114-2120.

862 81. Dobin A, Davis CA, Schlesinger F, Drenkow J, Zaleski C, Jha S, Batut P, Chaisson M, Gingeras TR. STAR:  
863 ultrafast universal RNA-seq aligner. *Bioinformatics*. 2013;29:15-21.

864 82. Li H, Handsaker B, Wysoker A, Fennell T, Ruan J, Homer N, Marth G, Abecasis G, Durbin R, Proc GPD.  
865 The Sequence Alignment/Map format and SAMtools. *Bioinformatics*. 2009;25:2078-2079.

866 83. Anders S, Huber W. Differential expression analysis for sequence count data. *Genome biology*.  
867 2010;11:R106.

868 84. Krueger F. Trim Galore. <https://github.com/FelixKrueger/TrimGalore>. Accessed 23 Juy 2021.

869 85. Yu GC, Wang LG, He QY. ChIPseeker: an R/Bioconductor package for ChIP peak annotation, comparison  
870 and visualization. *Bioinformatics*. 2015;31:2382-2383.

871 86. Carlson MM, B.P. TxDb.Athaliana.BioMart.plantsmart28: Annotation package for TxDb object(s).  
<https://bioconductor.org/packages/release/data/annotation/html/TxDb.Athaliana.BioMart.plantsmart28.html>. Accessed 7 Oct 2015.

872 87. Robinson JT, Thorvaldsdottir H, Winckler W, Guttman M, Lander ES, Getz G, Mesirov JP. Integrative  
873 genomics viewer. *Nature biotechnology*. 2011;29:24-26.

874 88. Jin Y, Ivanov M, Marquardt S. GSE186215.  
<https://www.ncbi.nlm.nih.gov/geo/query/acc.cgi?acc=GSE186215>. Accessed 20 Oct 2021.

880

**Fig. 1**

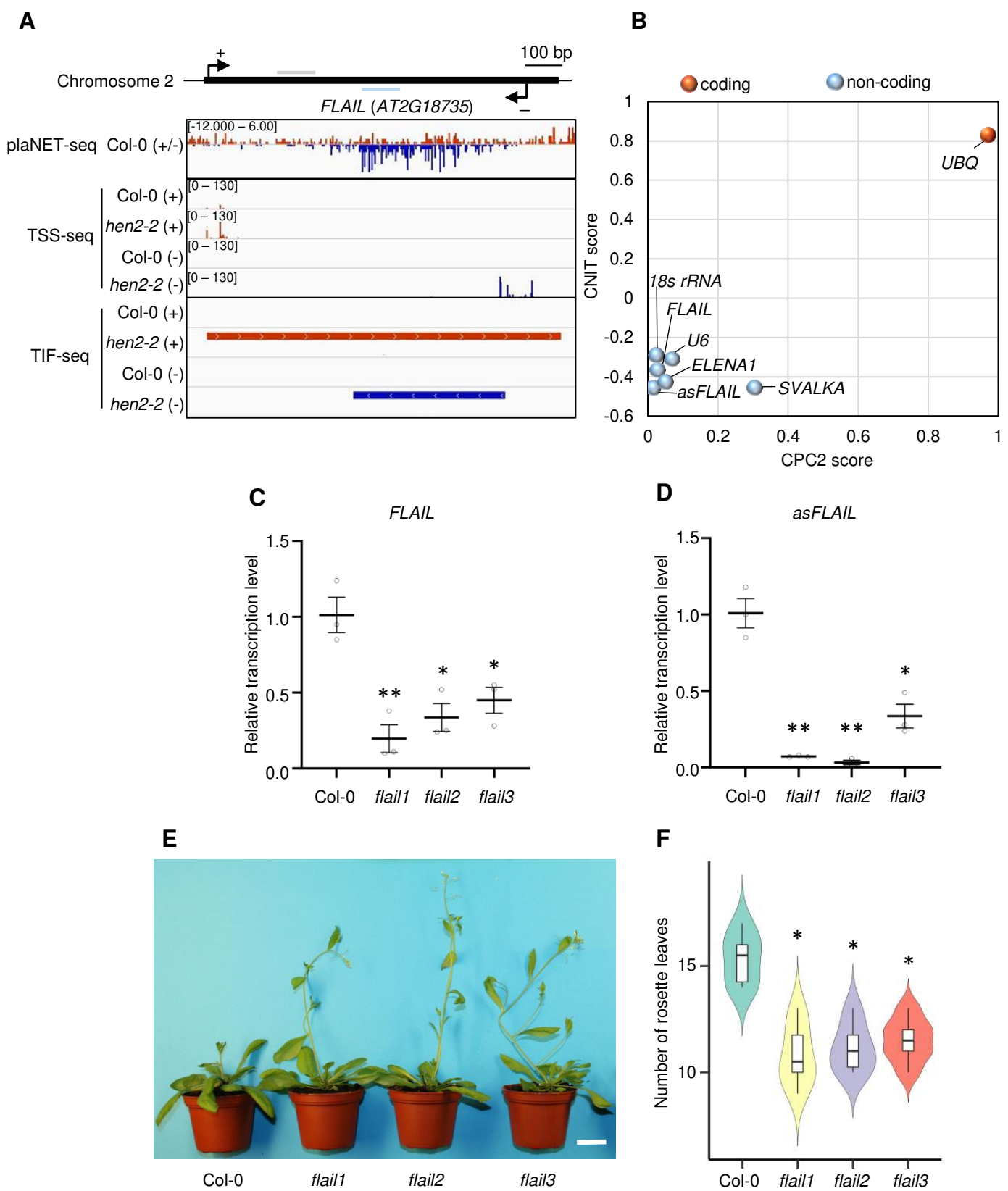


**Fig. 1** Phenotypes of *FLAIL* knock down plants. **A** Genome browser screenshot of plaNET-seq, TSS-seq and TIF-seq at the *FLAIL* genomic region in Col-0 and *hen2-2* mutant. Sense (+) and antisense (-) strands were shown in red and dark blue, respectively. Grey bar and light blue bar indicated primer locations of RT-qPCR for sense *FLAIL* (*FLAIL*) and antisense *FLAIL* (*asFLAIL*), respectively. **B** Coding potential of the transcript in the genomic region of *FLAIL* and *asFLAIL* and reference transcripts including non-coding RNAs (*18sRNA*, *U6*, *ELENA1*, *SVALKA*) and coding gene *UBQ* according to the CNIT and CPC2 algorithm. **C-D** Detection of *FLAIL* and *asFLAIL* gene expression in Col-0 and *flail* mutants by RT-qPCR. Transcript levels were normalized to *UBQ* expression levels. Y-axis showed relative values compared to the expression level of Col-0. Bars represented average  $\pm$  s.e.m (n = 3 independent 14-d seedling pools). \*, p value < 0.05 and \*\*, p value < 0.01 by Student's t-test compared to Col-0. **E** Morphological phenotypes of 4-week-old plants of Col-0, *flail* mutants at 20 °C under a 16-h light/8-h dark growth condition. Scale bar: 2 cm. **F** Violin graph showed number of rosette leaves after appearance of the first flower bud in Col-0. Data represented the mean of six independent experiments. Boxes spanned the first to third quartile, bold black lines indicated median value for each group and whiskers represented the minimum and maximum values. \*, p value < 0.05 was indicated by Student's t-test compared to Col-0.

**Fig. 2**

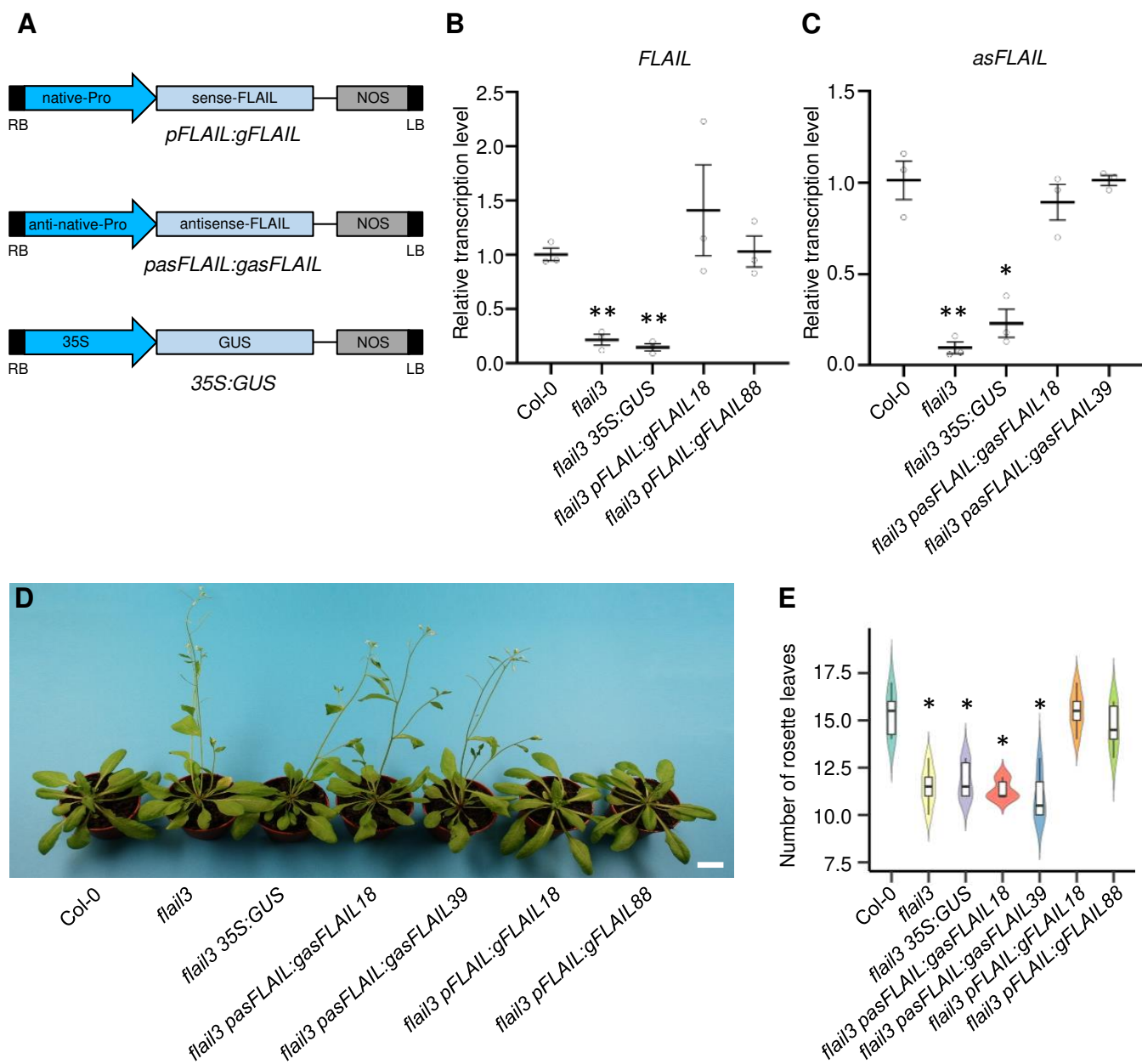


**Fig. 2 Sense-FLAIL mRNA is functional for flowering. A** Schematic representations of the T-DNA constructs containing the native promoter of *sense-FLAIL* (native-Pro) fused to the *sense-FLAIL* DNA region with NOS as a terminator or the native promoter of *anti-sense FLAIL* (anti-native-Pro) fused to the *anti-sense FLAIL* DNA region or a negative control with the 35S promoter (35S) fused to GUS reporter were transformed into *flail3* *Arabidopsis* plants. **B-C** Detection of *FLAIL* and *asFLAIL* genes expression in Col-0, *flail3* mutant and complemented lines expressing *pFLAIL:gFLAIL* and *pasFLAIL:gasFLAIL* by RT-qPCR. Transcript levels were normalized to *UBQ* expression levels. Y-axis showed relative values compared to the expression level of Col-0. Error bars represented s.e.m (n = 3 independent 14-d seedling pools). \*, *p* value < 0.05 and \*\*, *p* value < 0.01 by Student's t-test compared to Col-0. **D** Representative morphological phenotypes of 4-week-old plants of Col-0, *flail3* mutant, transgenic lines at 20 °C under a 16-h light/8-h dark growth condition. Scale bar: 2 cm. **E** Violin graph showed number of rosette leaves after appearance of the first flower bud in Col-0. Data represented the mean of six independent experiments. Boxes spanned the first to third quartile, bold black lines indicated median value for each group and whiskers represented the minimum and maximum values. \*, *p* value < 0.05 was indicated by Student's t-test compared to Col-0.

Fig. 3

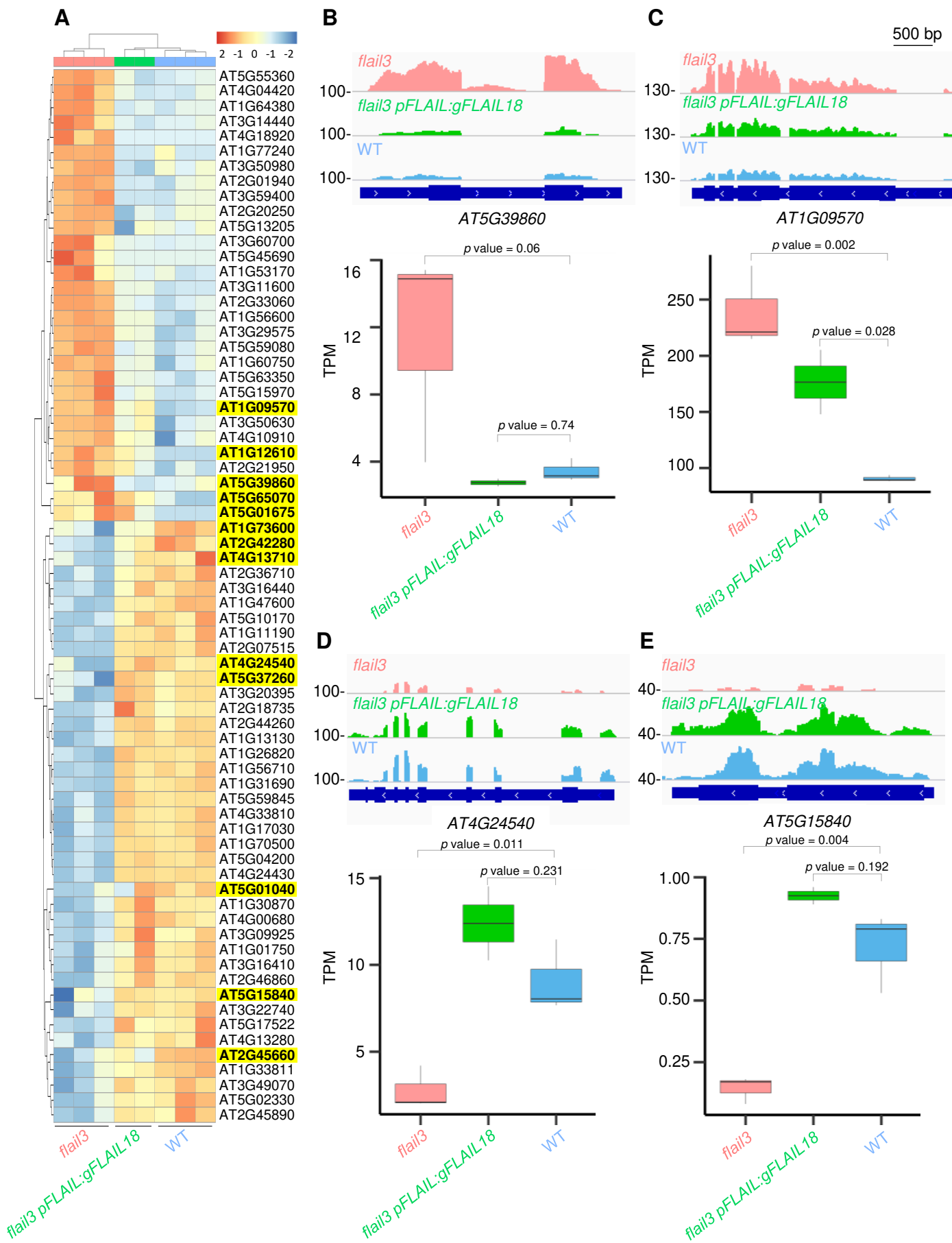


**Fig. 3** *FLAIL* regulates flowering related genes. A Heatmap and hierarchical clustering of top

70 differentially expressed genes (DEGs) in *flail3* versus Col-0 that were best rescued in the *flail3 pFLAIL:gFLAIL18* complementation line. DEGs analyzed by DESeq2 with  $|\log_2 \text{fold change}| > 1$  and adjusted  $p$  value  $< 0.05$  were considered significant differential expression. Three biological replicates for *flail3*, wild type, and two for *flail3 pFLAIL:gFLAIL18*. Flowering genes were highlighted in yellow bold. Samples clustered together on the basis of corresponding similar expression profiles. The color scale reflected the log 2-fold change in gene expression, ranging from down-regulated (blue) to up-regulated (red). **B-E** Genome browser screenshots illustrating the expression of dysregulated flowering genes in *flail3* were rescued in complementation line (top panel). Normalized read counts (TPM from RNA-seq) for differentially expressed flowering genes in WT, *flail3*, and *flail3 pFLAIL:gFLAIL18* plants (bottom panel). Boxes spanned the first to third quartile, bold black lines indicated median value for each group and whiskers represented the minimum and maximum values. All  $p$  values were denoted by Students' t-test. Bar = 500 bp.

**Fig. 4**

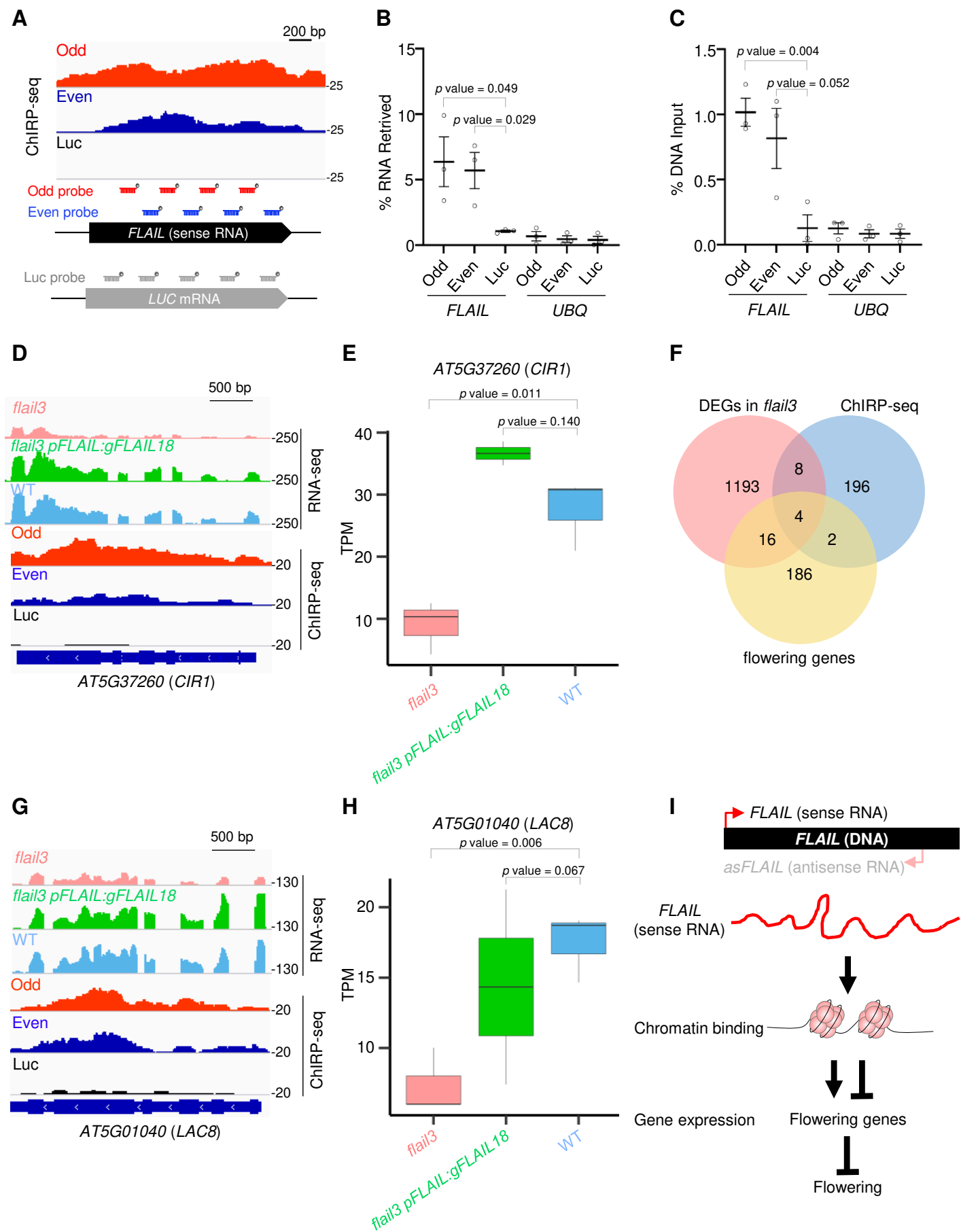


**Fig. 4** *FLAIL* affects flowering by chromatin binding of flowering genes. **A** Top, *FLAIL* bound the locus itself by ChIRP-seq from two independent Odd and Even probed chromatins. Luc probe was used as a control. Bottom, schematic representation of the antisense oligonucleotide probes that were biotinylated at the 3'-end with Odd (in red) and Even (in dark blue) against *FLAIL* sense RNA and Luc probe (in grey) against *LUC* mRNA. **B** ChIRP-qPCR using probe pools *FLAIL*-asDNA (Odd and Even) retrieved ~5%–10% of *FLAIL* endogenous RNA and < 1% levels of *UBQ*. *Luc*-asDNA probes retrieved much lower levels of both RNAs as a control. **C** *FLAIL* DNA signal was identified in both Odd and Even probes. *UBQ* region showed much less binding signal in all probes as a negative control. Graphs in **B** & **C** showed the mean  $\pm$  s.e.m. (n= 3 independent replicates). **D**, **G** Genome browser screenshots illustrating two of *FLAIL* bound targets *CIR1* (**D**) and *LAC8* (**G**) in RNA-seq (lane 1-3) and ChIRP-seq (lane 4-6). *FLAIL* binding peaks were called by CCAT3.0 with the cutoff FDR = 0.232. **E**, **H** Normalized read counts (TPM from RNA-seq) for differentially expressed (DE) flowering genes in WT, *flail3*, and *flail3 pFLAIL:gFLAIL18* plants (bottom panel). Boxes spanned the first to third quartile, bold black lines indicated median value for each group and whiskers represented the minimum and maximum values. **F** Venn diagram of genes targeted by *FLAIL* (ChIRP-seq) and genes overlapped with DEGs in *flail3* and flowering related genes. **I** A model for the *trans*-acting *FLAIL* sense RNA regulated flowering. The *FLAIL* sense RNA binds chromatin regions of flowering genes to regulate expression levels of flowering related genes and thus affects flowering time. All *p* values were denoted by Students' t-test.

**Fig. S1**

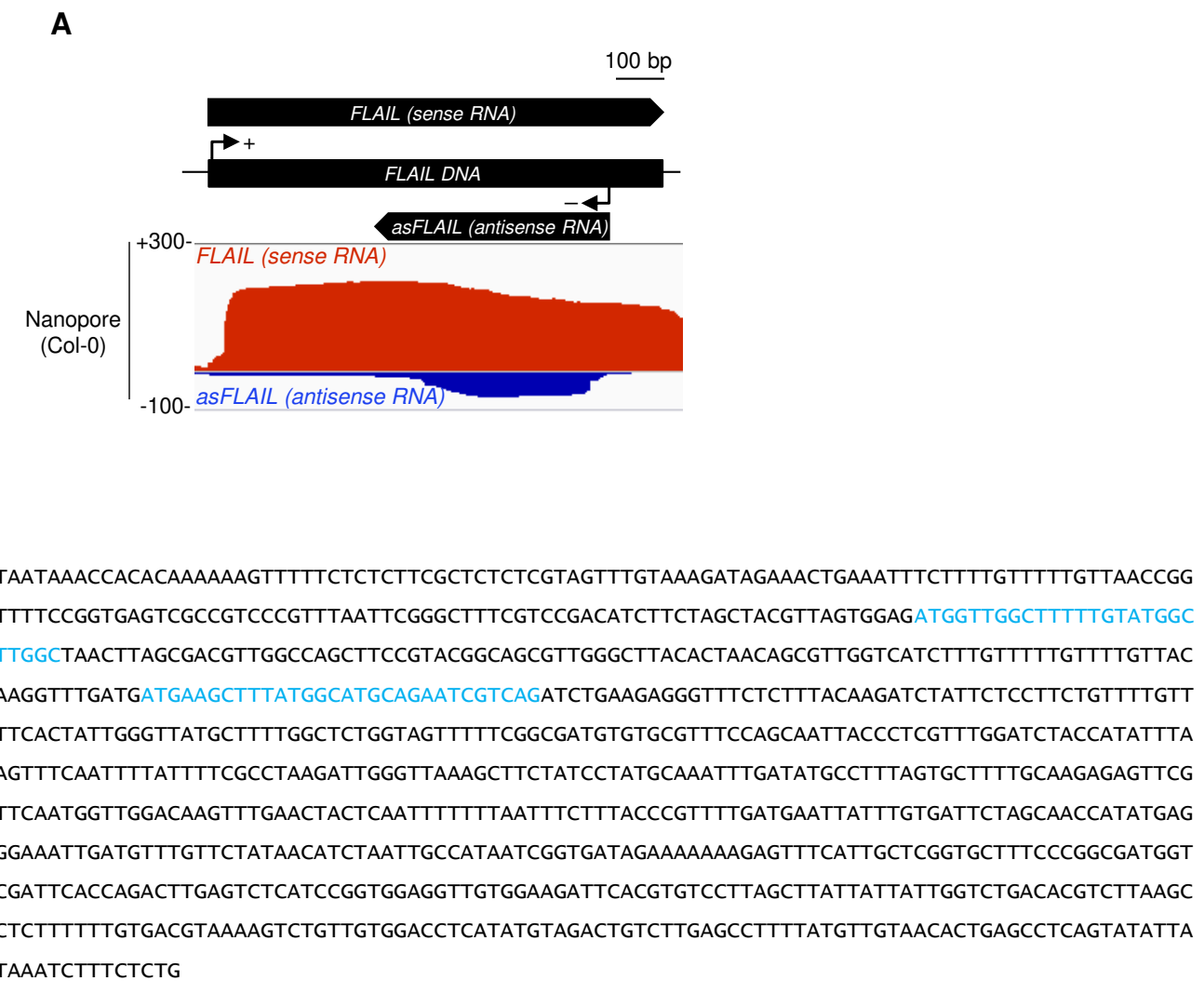


**Fig. S1** Characterization of *FLAIL* locus. **A** Genome browser view of *FLAIL* splicing status in nanopore sequencing of Col-0. Transcription of sense *FLAIL* RNA and *asFLAIL* RNA were shown in red and dark blue, respectively and no isoform resulting from alternative splicing was observed. **B** *FLAIL* nucleotide sequences in black and two sORFs locations in blue.

Fig. S2

## NetStart Prediction

Name: FLAIL  
AAGTTAAATACCAACACAAAAAAGTTTTCTCTCTTCG  
CTCTCTCGTAGTTGAAAGATAGAAACTGAAATTCT  
TTGGTTTTGTTAACCGGATAGTTTCCGGTAGCTGC  
CGTCCCGTTAATTCGGGCTTCGTCGACATCTCTA  
GCTACGTTAGTGGAGATGGTTGGCTTTGTATGGCAT  
CGTGGCTAACTAGGGACAGTGGCCAGCTTCCGACG  
CGAGCGGGCTTGGGCTTACACTAACAGCGTGGCTAC  
GTTTTGTTTGTACTCAAAGGTTGATGATGAAAGC  
TTTATGGCATCGAGAACATGCTGACATCTGAAAGGTTT  
CTCTTACAAAGATCTTCTCTCTGTTTGTGTTAGC  
TTCACTATGGGTTATGCTTTGGCTCTGGTAGTTT  
CGGCAGTGTGCGTTCCAGCAATTACCCCTGGTTGG  
ATCTACCATATTAAAGACAGCTTCAATTATTTTGGC  
CTAAAGATTGGTTAAAGCTTCTATCTTCAAAATTG  
ATATGCCTTAGTGTGTTGCAAGAGAGTCTGAAGATT  
CAATGTTGGACAAGTTGAACTACTCAATTTTTTAA  
TTCTTACCCGGTTGGATGAAATTATTTGTGATTCAG  
CAACATTAGGATTAGGAAGATTGATGTTGTTCTATA  
ACATCTAATTGCCATAATCGGTGATAGAAAAAAAGT  
TTCACTGGTCGGTCTTCCGGCGATGGTTCTCGAT  
TCACCAAGACTGAGTCATCCTGGAGGTTGGAA  
GATTACCTGGCTCTTGGCTTATTTTGTGACGCTGACA  
CGTCTTAAGCTTATCTCTTTTGTGACGTTAAAGTCT  
GTTGGACCTCATATGAGACTGTCCTGAGCCCTTTA  
TGTGTAACACTGAGCTCAGTATATTAAAAAATAATC  
TTCTCTG

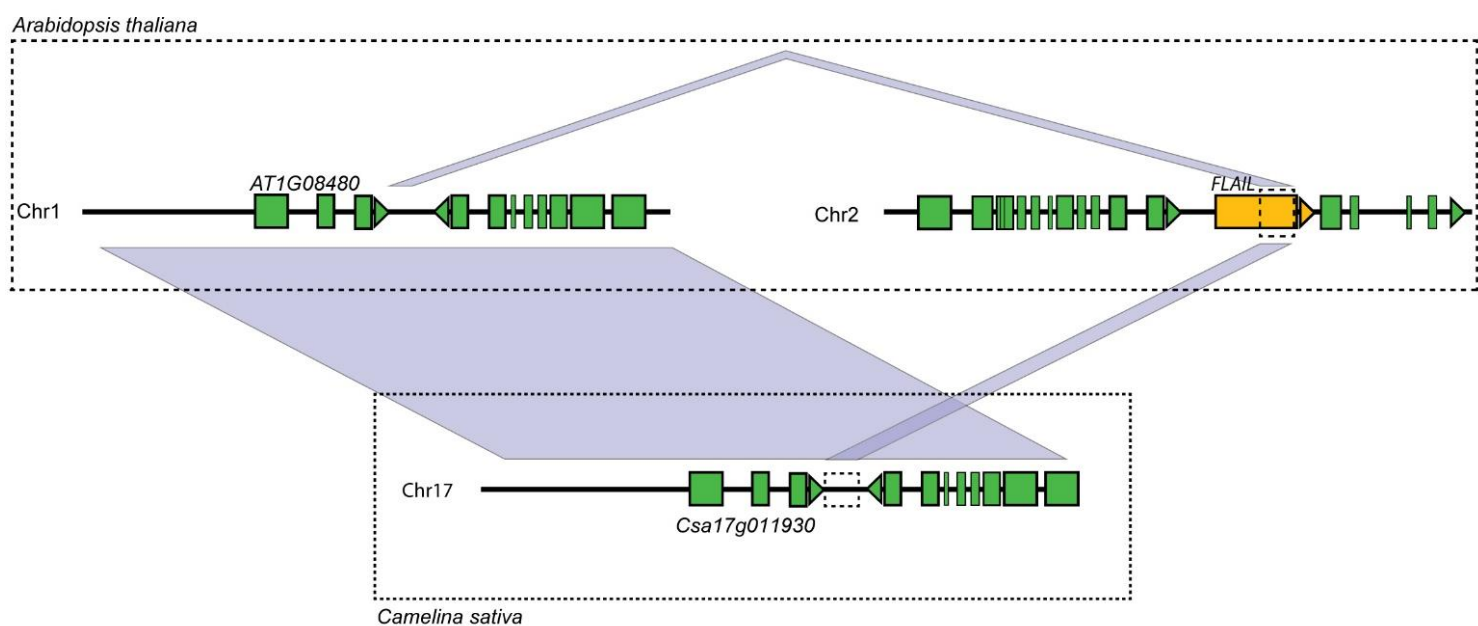
i.....N.  
.....i.....N.  
.....N.....N.  
.....i.....N.....N.  
.....N.....N.....N.....N.

Pos	Score	Pred	Pos	Score	Pred
168	0.419	-	583	0.718	Yes
184	0.218	-	737	0.265	-
295	0.106	-	811	0.543	Yes
298	0.149	-	965	0.126	-
308	0.366	-	1839	0.471	-
313	0.287	-	1193	0.355	-
395	0.318	-	1267	0.549	Yes
424	0.324	-	1421	0.257	-
522	0.290	-	1495	0.537	Yes
535	0.346	-	1649	0.192	-
573	0.305	-	1723	0.667	Yes
626	0.262	-	1877	0.200	-
654	0.199	-	1971	0.188	-
671	0.443	-	1987	0.057	-
748	0.208	-	1999	0.152	-
889	0.080	-	2046	0.181	-
912	0.048	-	2064	0.345	-
			2096	0.241	-
			2242	0.100	-
			2277	0.111	-
			2288	0.054	-
			2312	0.042	-
			2315	0.038	-

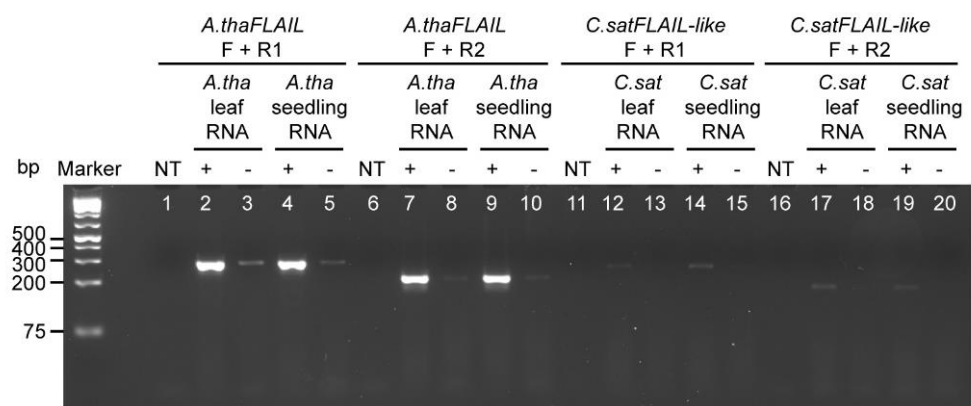
**Fig. S2** Assessment of *FLAIL* and *UBQ* for protein coding potential. Initiation codon translational analysis using NetStart for *FLAIL* and *UBQ*. The predicted initiation codons were depicted with the letter i, other instances of "ATG" by the letter "N" (non-start). The dots (".") were place holders for all the other sequence elements. The scores were always in [0.0, 1.0]; when greater than 0.5, they represented a probable translation start.

**Fig. S3**

**A**



**B**



**C**

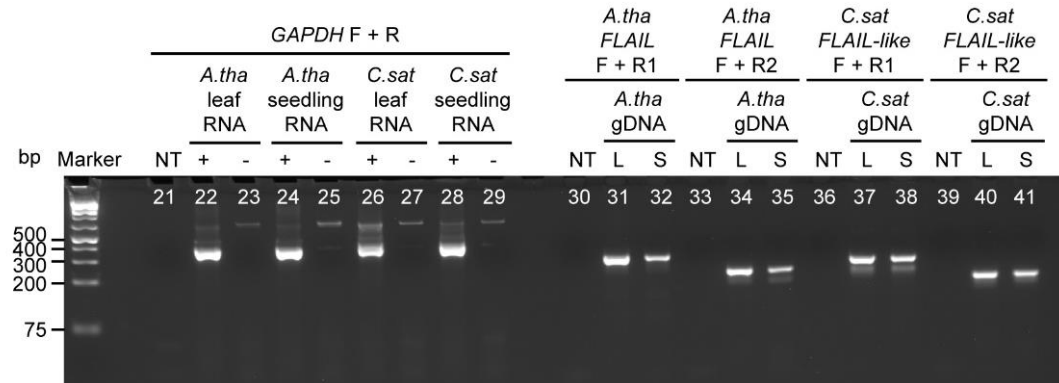


**Fig. S3** Sequence and transcriptional conservation at the *FLAIL* and *FLAIL-like* loci in *Arabidopsis* and *Camelina*. **A** Schematic depicting the conservation of the *Arabidopsis* (*A.tha*) *FLAIL* locus in *Camelina sativa* (*C.sat*). Green boxes represent exons, with triangles representing direction of transcription. The *FLAIL* locus is represented by a yellow box. Faded blue lines represent sequence similarity between different loci. Dashed boxes at the *FLAIL* and *Csa17g011930* loci represent regions targeted for RT-PCR. **B** Amplification of *A.thaFLAIL* and *C.satFLAIL-like*, using RNA template (+/- RT, lanes 1-20). NT indicates no template was added to the reaction. **C** Control amplifications: *GAPDH* was amplified using RNA template (+/- RT, lanes 21-29), and *A.thaFLAIL* and *C.satFLAIL-like* were amplified using genomic DNA template (lanes 30-41). L indicates leaf tissue, S indicates seedling tissue.

**Fig. S4**

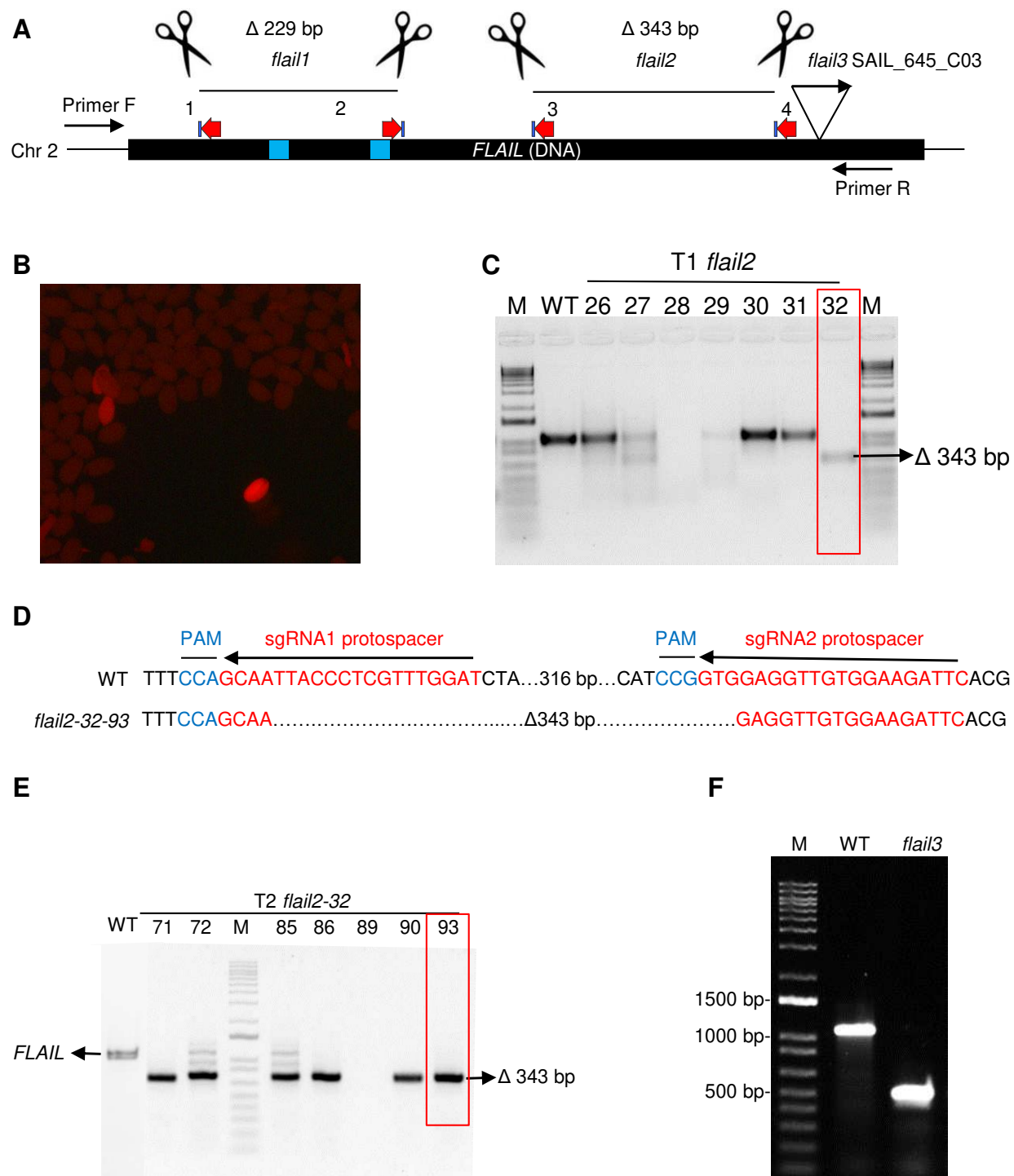
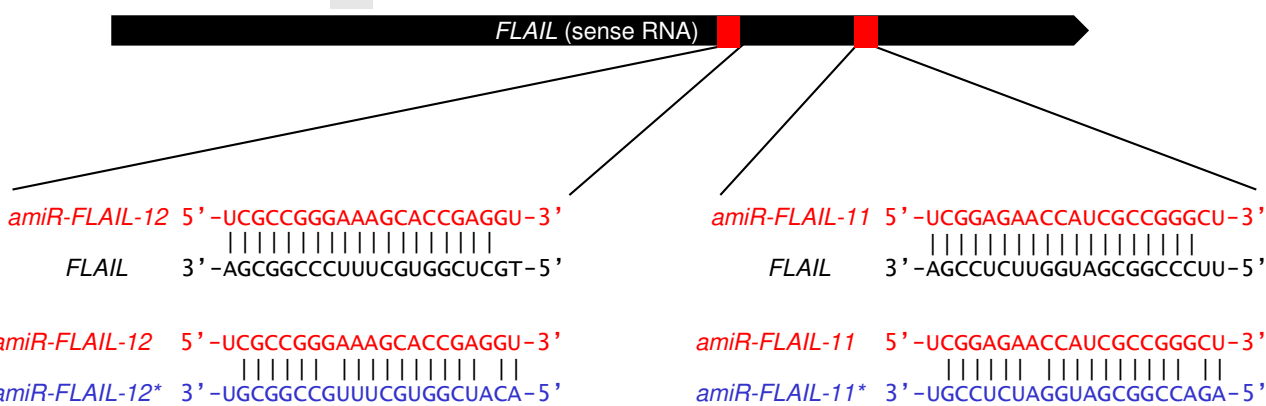


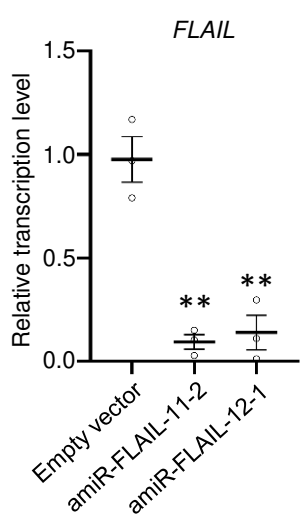
**Fig. S4** *FLAIL* dual-sgRNA approach and T-DNA insertion genotyping. **A** Schematic representation of targeted gene *FLAIL* with locations of two Cas9-directed mutants *flail1*, *flail2*, and one T-DNA mutant *flail3*. Locations of dual-sgRNA target sites were shown in red arrow, primer pair F/R (Mlo2478/2479) were used for PCR testing deletion in *flail1* and *flail2*, triangle indicated the putative position of T-DNA insertion at the *FLAIL* locus. Blue boxes indicated two sORFs. **B** Similar to the previous generation of *flail1*, *FLAIL2* construct containing pKIR1.1 enabled red fluorescence selection of *flail2* seeds from T1 plants after transformation by floral dipping. **C** Genotyping of individual T1 plant with red fluorescence, Leaf genomic DNA of T1 plants were PCR amplified. Expected size of PCR product for deletion was 343 bp in *flail2* line. *flail2-32* in red box was selected for next generation. **D** In T2 selection, the null mutant *flail2-32-93* without red fluorescence in seeds represented Cas9-free plants, indicated by red box in **E**. PAM was shown in blue, sgRNA protospacers were in red, and deleted bases were replaced by dots. **F** PCR analysis of T2 lines. The expected size of the wild-type *FLAIL* amplicon and the deletion size between Cas9 cut sites in *flail2-32-93* were indicated. This inherited Cas9-null segregation line was used for data analysis in Fig. 1. **G** Genotyping of the T-DNA insertion mutant *flail3*. Gel sample order (from left to right): lane 1, marker; lane 2, WT; lane 3, *flail3*, with primer set, Mlo1788 + Mlo1789 + Mlo37; Results clearly showed that *flail3* line was homozygous since WT was the only line giving WT band and *flail3* line gave the only T-DNA insertion band.

**Fig. S5**

**A**



**B**



**C**



**D**

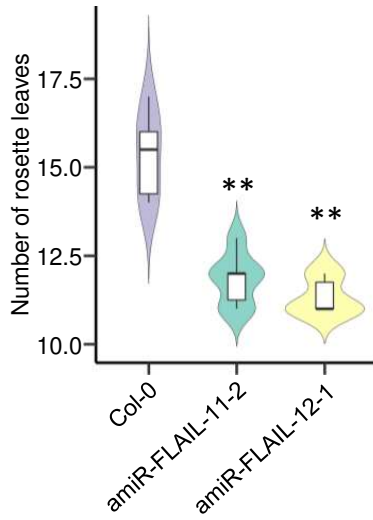


**Fig. S5** *FLAIL* lncRNA functions as a flowering repressor. **A** Sequences and structures of amiRNA duplexes and the target sites of *amiR-FLAIL*s and *amiR-FLAIL*\*s. Upper panel, schematic representation of transcribed sense *FLAIL* RNA. Lower panel, sequences of amiRNA duplexes, amiRNA (in red) target sites, and potential amiRNA\* (in blue) on cognate sense *FLAIL* (in black). **B** Gene expression of sense *FLAIL* in *amiR-FLAIL* plants by RT-qPCR. Transcript levels were normalized to *UBQ* expression levels. Two representative lines for amiRNA designed transgenic plants were selected. Y-axis showed relative values compared to the expression level of empty vector transformed plants. Grey bars depicted the relative positions of primers used for RT-qPCR analyses. Transcript levels were normalized to *UBQ* expression levels. Error bars represented s.e.m (n = 3 independent 14-day seedling pools). \*\*, p value < 0.01 analyzed by Student's t-test. **C** Morphological phenotypes of 4-week-old plants of Col-0 and two *amiR-FLAIL* plants under a 16-h light/8-h dark growth condition. Scale bar: 2 cm. **D** Violin graph showed number of rosette leaves after appearance of the first flower bud in Col-0. Data represented the mean of six independent experiments. Boxes spanned the first to third quartile, bold black lines indicated median value for each group and whiskers represented the minimum and maximum values. \*\*, p value < 0.01 was indicated by Student's t-test compared to Col-0.

**Fig. S6**

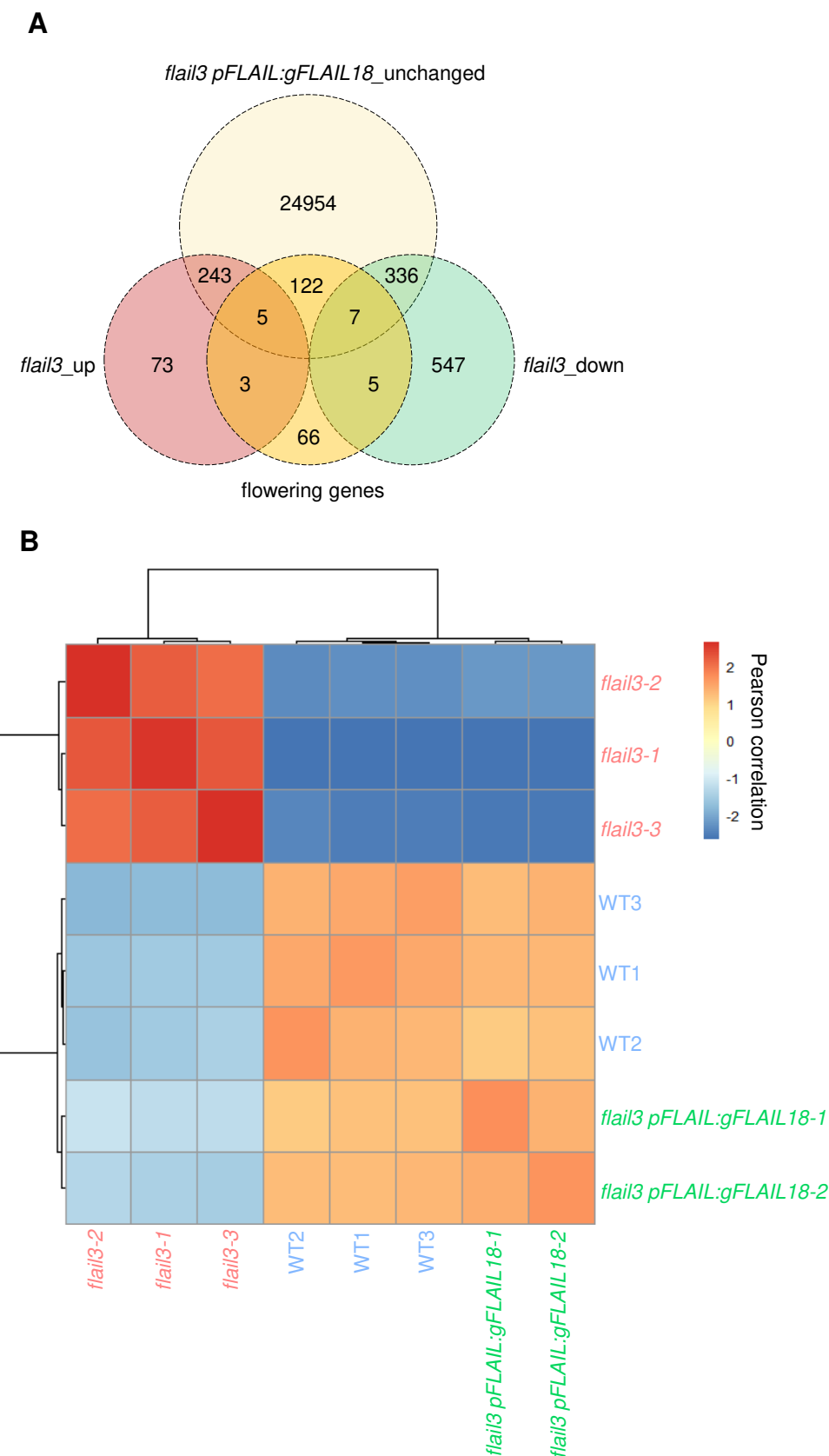


**Fig. S6** Genome-wide effects of *FLAIL* on gene expression by RNA-seq. **A** Venn diagram of flowering genes overlapped with upregulated and downregulated genes in the *flail3* mutant and with unchanged genes in the *flail3 pFLAIL:gFLAIL18* complementation plant. **B** Reproducibility of all genes shown in Fig. 3 from RNA-seq data was demonstrated by clustered heatmap of Pearson correlation coefficients over all independent replicates of RNA-seq in WT, *flail3* mutant, and *flail3 pFLAIL gFLAIL18* plants. Darker red denoted higher correlation and darker blue represented low reproducibility.

**Fig. S7**

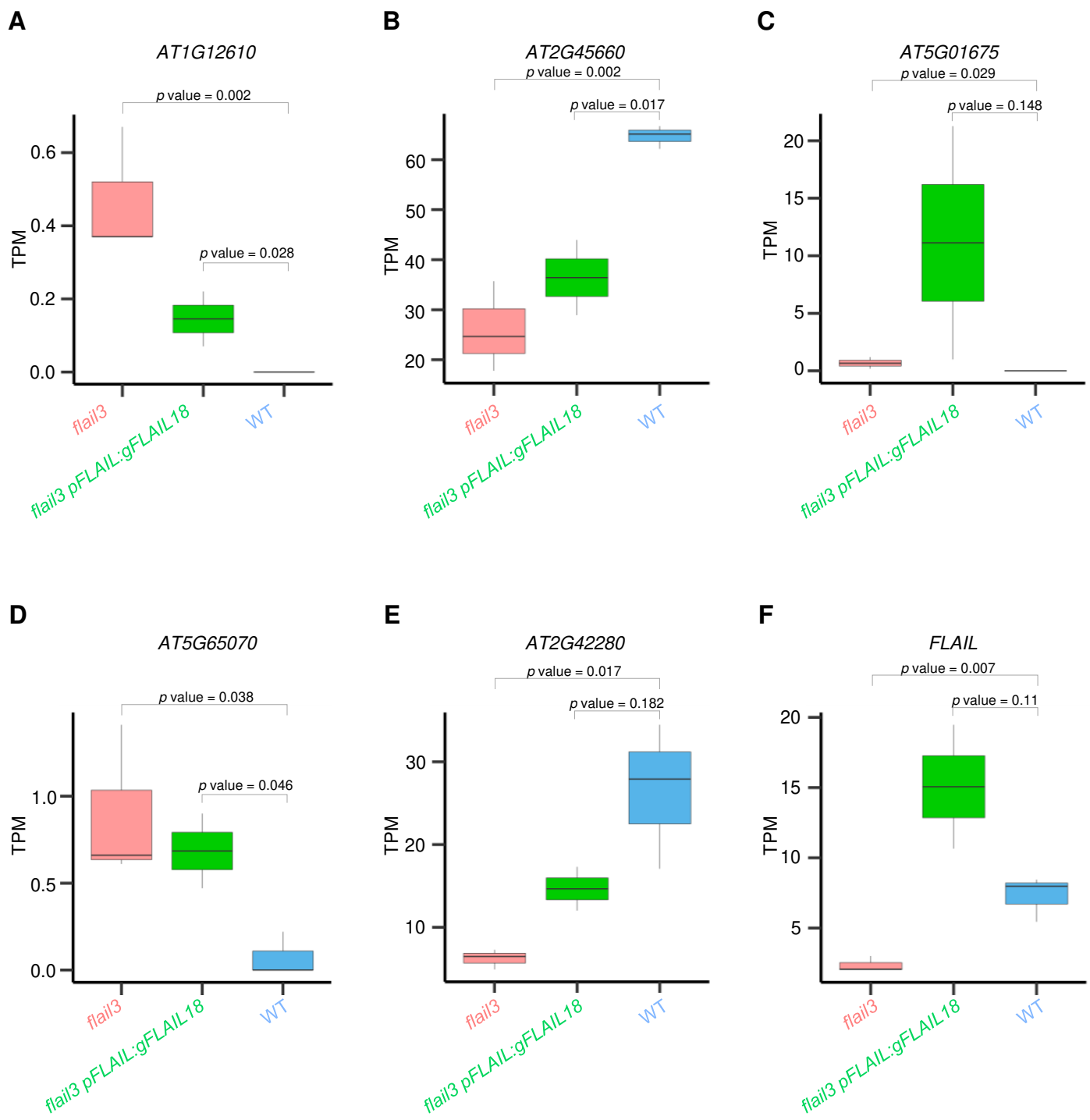


**Fig. S7** *FLAIL* regulates flowering related genes in *trans*. **A-F** Genome browser screenshots illustrating the expression of dysregulated flowering genes in *flail3* were most fully rescued in complementation line. Normalized read counts (TPM from RNA-seq) were used for differentially expressed flowering genes in WT, *flail3*, and *flail3* *pFLAIL:gFLAIL18* plants. Boxes spanned the first to third quartile, bold black lines indicated median value for each group and whiskers represented the minimum and maximum values. *p* value was denoted by Students' t-test.

**Fig. S8**

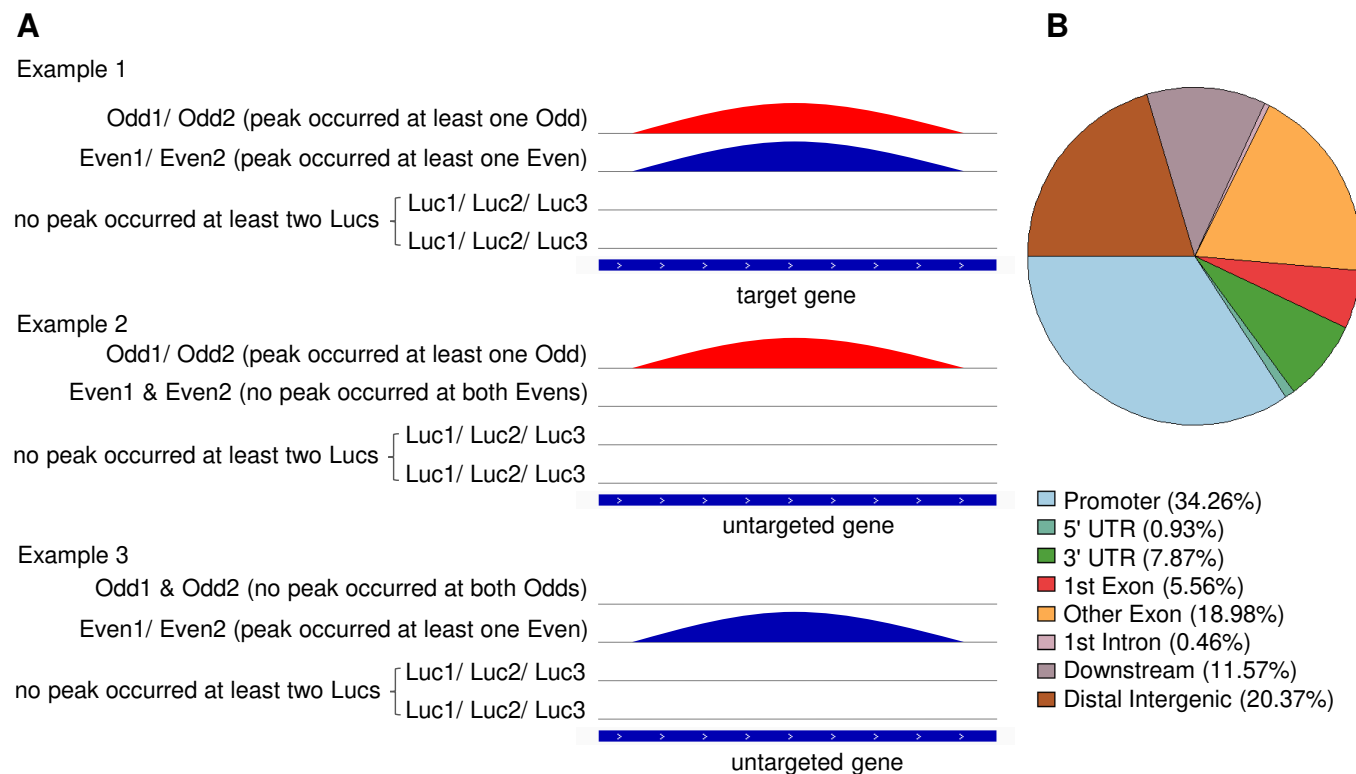


**Fig. S8** Strategy to identify genome-wide binding profile of *FLAIL* analyzed by ChIRP-seq. **A** Illustration of *FLAIL* peaks called by CCAT3.0. Only peaks that occurred at target genes from both Even and Odd probed DNA, but not from two or more independent experiments of Luc pools were considered significant enrichment (Example 1), peaks that only occurred from either Even or Odd pools were not considered *FLAIL* targets (Example 2 & 3). **B** A pie chart that was generated by ChIPseeker represented distribution of *FLAIL* bound regions in the genome. A total of 210 *FLAIL* bound regions were annotated according to the genomic distribution and *FLAIL* was enriched predominantly in promoter regions.

**Fig. S9**

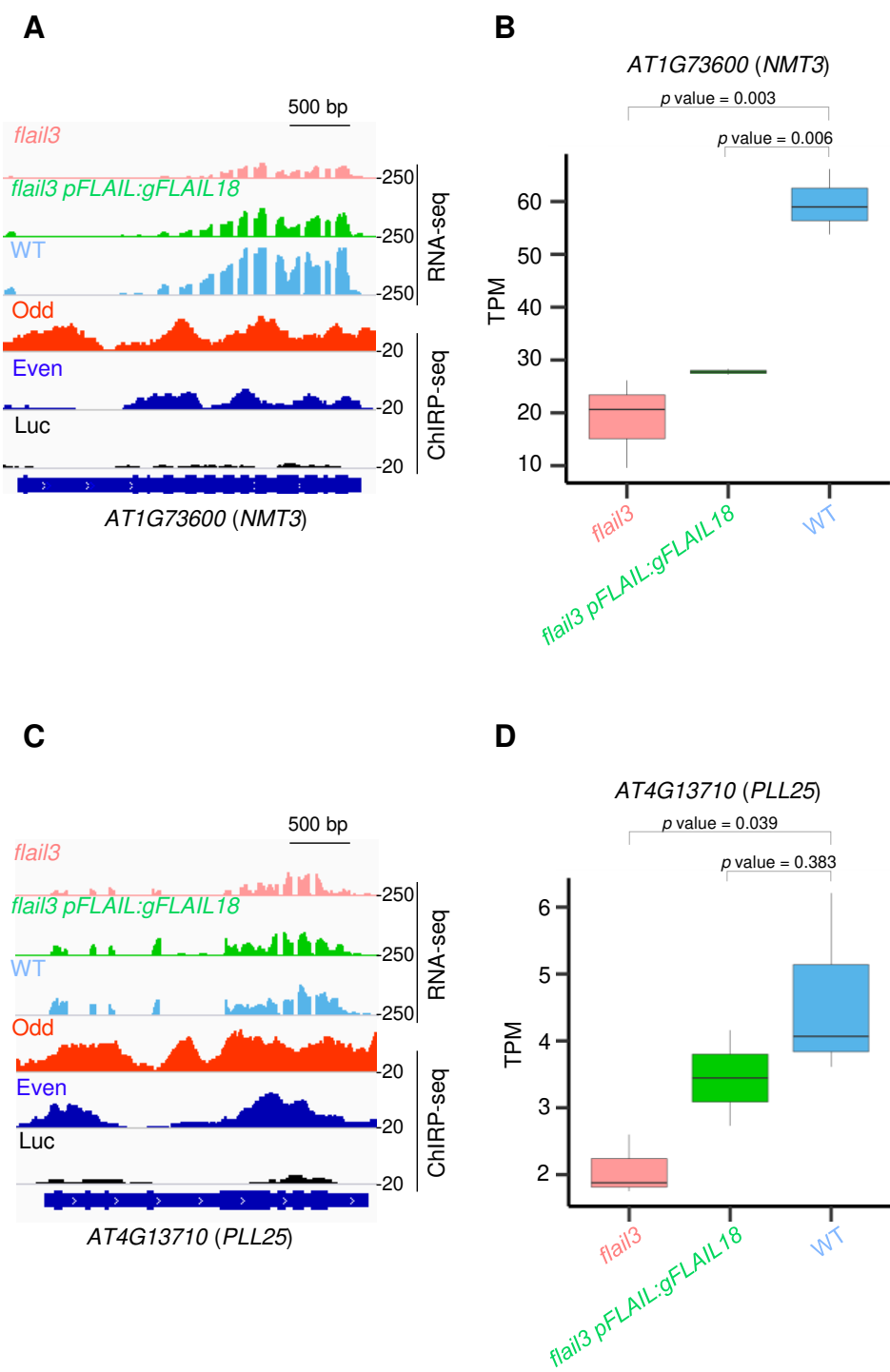


**Fig. S9** *FLAIL* binds chromatin regions of flowering genes for gene regulation. **A, C** Genome browser screenshots illustrating two more *FLAIL* bound flowering targets *PLL25* and *NMT3* in RNA-seq (lane 1-3) and ChIRP-seq (lane 4-6). Their expression that was downregulated in *flail3* (lane 1) can be partially or fully rescued in complementation line (lane 2). Both Odd and Even probes identified chromatin binding regions of *FLAIL* in two more flowering genes *NMT3* and *PLL25* compared to *Luc* probes. *FLAIL* binding peaks were called by CCAT3.0. **B, D** Normalized read counts (TPM from RNA-seq) for differentially expressed (DE) flowering genes in WT, *flail3*, and *flail3 pFLAIL:gFLAIL18* plants (bottom panel). Boxes spanned the first to third quartile, bold black lines indicated median value for each group and whiskers represented the minimum and maximum values. *p* value was denoted by Students' t-test.

**Fig. S10**

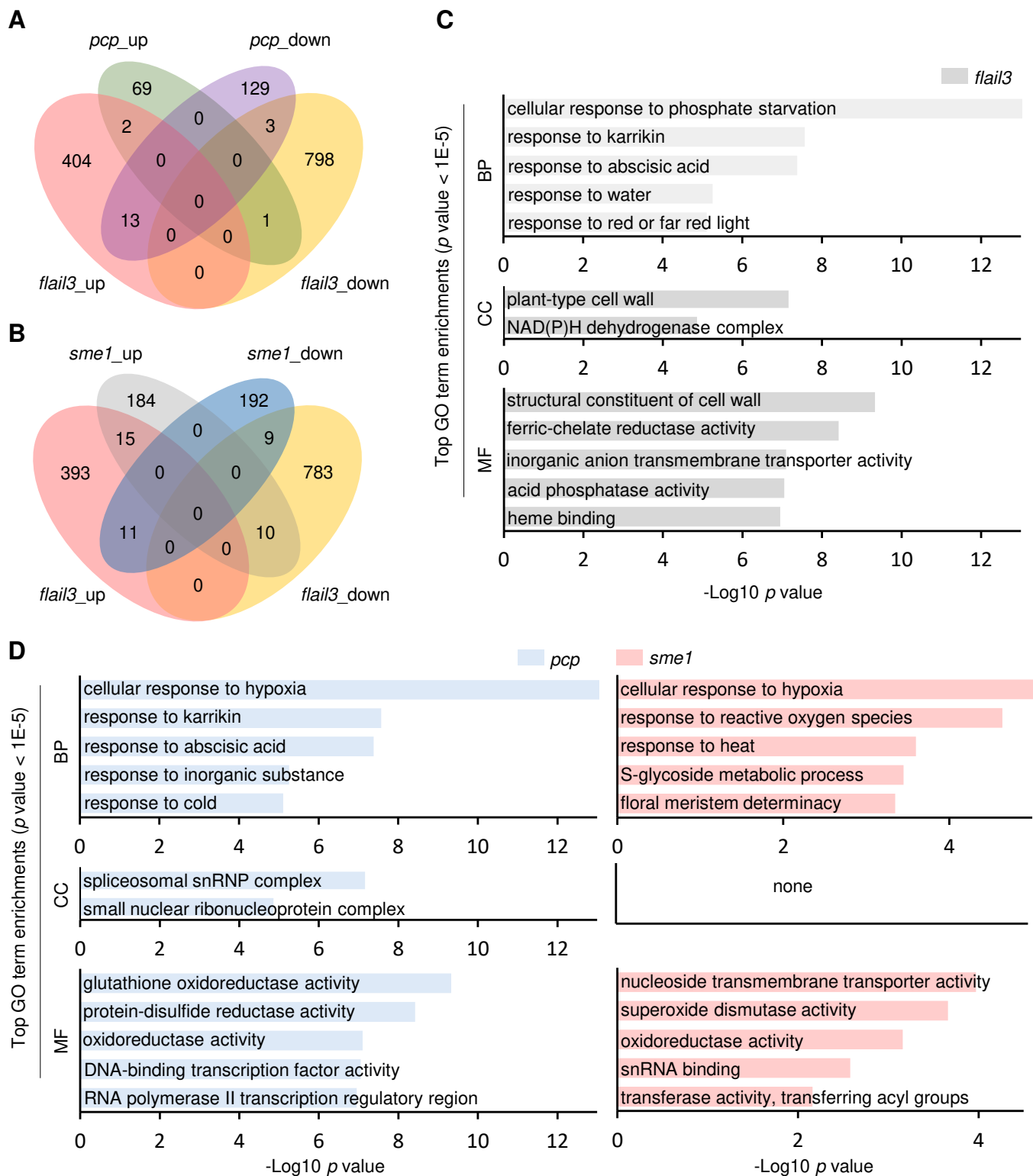


**Fig. S10** *FLAIL* regulates flowering independent of *PCP*. **A, B** Venn diagram showing overlapping differentially expressed genes (up/down) sets between *flail3* and *pcp* (also called *sme1*) mutants. **C, D** GO analysis of the DEGs in RNA-seq data of *flail3* and *pcp* /*sme1* mutants. Y-axis indicated the GO categories including biological process (BP), cellular component (CC) and molecular function (MF); X-axis showed -Log10 p value with the cutoff 0.05. Highly enriched GO terms of dysregulated mRNAs analyzed by the Metascape with 5 top enrichment scores.